

DESIGN AND DEVELOPMENT OF AN EMC ANTENNA FOR
ON-LINE PLANE WAVE SHIELDING EFFECTIVENESS
MEASUREMENT OF A PLANAR SHEET

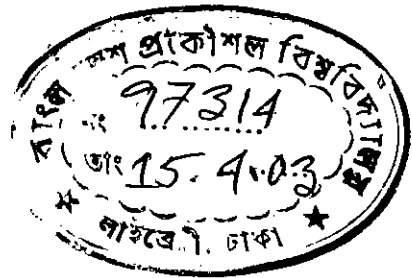
A Thesis

Submitted to the Department of Electrical and Electronic Engineering, BUET, Dhaka in
partial fulfillment of the requirements for the degree

of

MASTER OF SCIENCE IN ELECTRICAL AND ELECTRONIC ENGINEERING

by



PRABAL KANTI DAS

DEPARTMENT OF ELECTRICAL AND ELECTRONIC ENGINEERING
BANGLADESH UNIVERSITY OF ENGINEERING AND TECHNOLOGY
DHAKA, BANGLADESH

April, 2003



#97314#


Dedicated to my parents

Mr. Sadhan Bikash Das
&
Mrs. Renu Prava Das

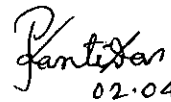
CERTIFICATE

This is to certify that the work presented in this thesis was done by me under the complete supervision of **Dr. Pran Kanai Saha**, Professor, Department of Electrical and Electronic Engineering, BUET, Dhaka, Bangladesh. It is also certify that this thesis work has not been submitted for the award of any degree or diploma.

Countersigned:



(Dr. Pran Kanai Saha)


02.04.2003

(Prabal Kanti Das)

The thesis titled “**DESIGN AND DEVELOPMENT OF AN EMC ANTENNA FOR ON-LINE PLANE WAVE SHIELDING EFFECTIVENESS MEASUREMENT OF A PLANAR SHEET**”, submitted by Prabal kanti das, Roll No. 9506208P, Registration No. 9506208, Session 1994-95-96 of M. Sc. in Engineering has been accepted as satisfactory in partial fulfillment of the requirements for the degree of

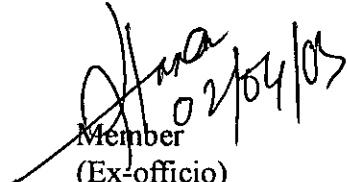
MASTER OF SCIENCE IN ELECTRICAL AND ELECTRONIC ENGINEERING

Board of Examiners

1. **DR. PRAN KANAI SAHA**
Professor
Department of Electrical & Electronic Engineering,
BUET, Dhaka-1000.


Chairman
(Supervisor)

2. **DR. M.M. SHAHIDUL HASSAN**
Professor and Head
Department of Electrical & Electronic Engineering,
BUET, Dhaka-1000.


Member
(Ex-officio)


3. **DR. SATYA PRASAD MAJUMDER**
Professor
Department of Electrical & Electronic Engineering,
BUET, Dhaka-1000


Member

4. **DR. MD. SHAH ALAM**
Assistant Professor
Department of Electrical & Electronic Engineering,
BUET, Dhaka-1000.


Member

5. **DR. NUR MAHABUBUL ALAM CHOWDHURY**
Assistant Professor
Department of Electrical & Electronic Engineering,
BIT, Dhaka, Gazipur-1700.


Member
(External)

ACKNOWLEDGEMENT

The author would like to acknowledge his sincere and profound gratitude to his advisor, Dr. Pran Kanai Saha who patiently gave many invaluable advises, continuous guidance and constant encouragement during thesis work.

The author takes the opportunity to express his deepest appreciation to Dr. M.M. Shahidul Hassan, Professor and Head of the Department of Electrical and Electronic Engineering, BUET for providing departmental facilities. The author gratefully acknowledges for the research grants provided by the authority of BUET that enable the author to conduct this research.

Special thanks to Dr. Md. Kamrul Hasan, Associate Professor, Department of Electrical & Electronic Engineering, BUET for his cooperation in getting the experimental results.

Finally, author would like to give thanks to them who directly or indirectly helped in this research work, specially, to Md. Abul Qashem Bhuiayn, Chief Engineer, National Broadcasting Authority, Bangladesh Betar (NBAB), Md. Mizanur Rahman, Resident Engineer, High Power Transmitting Station (HPTS)-1, Bangladesh Betar, Md. Manirul Islam, Station Engineer, Bangladesh Betar, Engr. A.K.A.M. Fazlul Hoque, Bangladesh Betar, Engr. Md. Masud Bhuiyan, Bangladesh Betar, Engr. Ranjit Kumar Mandal, Bangladesh Betar, Engr. Foezur Rahman Chowdhury, Bangladesh Betar for their encouragement to do this thesis work.

ABSTRACT

The electromagnetic environment has become polluted because of widespread proliferation of various electronic appliances and instruments in our daily life. The emergence of micro-processors, micro-controllers and miniaturization of high speed computers along with the development of telecommunication EMC has gained a paramount importance. The EMC studies both reflect and promote the awareness among the designers and manufacturers of electronic equipment of the need to combat Electromagnetic Interference (EMI) from both inter- and intra devices. The EMI from a equipment can be controlled or minimized by enclosing the equipment with a conductive shielded enclosure.

This research work is aimed at designing and developing frequency independent antenna for plane wave Shielding Effectiveness (SE) measurement of planar sheet like conductive composite materials during a continuous production cycle. There is a necessity of an EMC antenna namely, V-Conical Lens Antenna for on-line SE measurement. So, V-Conical Lens Antenna (VCLA) is designed and developed. A pair of VCLA is used where one acts as transmitting antenna and the other acts as receiving antenna to measure the SE. The size of the antenna is chosen chiefly by the sheet width of the Material Under Test (MUT). The feeding arrangement of the VCLA is such that the centre stud of the co-axial N-connector can be employed as a monopole antenna protruding into the cone to feed it. A plano-convex lens is used for VCLA and the lens is designed and constructed on the basis of Fermat's principle by nylon.

The field pattern, gain and directivity of the newly developed EMC antenna is computed and measured. It is observed that the directivity and gain of the antenna is higher than any other EMC antenna. Moreover, the gain of the developed antenna is constant over a frequency range 300MHz – 600MHz. That is why it signifies as a frequency independent antenna with in the mentioned frequency range. The pattern of the antenna is also consistent with the theoretical pattern except some weak field in the shadow region. This

may due to non-standard test environment. Lack of open site location and anechoic chamber are the additional factors to influence the measurement. That is why the measured SE values of different types of planar sheet like materials are varied with the theoretical results.

CONTENTS

	Pages
Certificate	(iii)
Board of Examiners	(iv)
Acknowledgment	(v)
Abstract	(vi)
List of Acronyms	(xi)
List of Symbols	(xii)
List of Figures	(xiii)

CHAPTER 1 ELECTROMAGNETIC COMPATIBILITY

1.1	Introduction	1
1.2	Shielding Materials	2
1.3	Measurement of Shielding Effectiveness	4
1.4	Benefits of On-line SE Measurement	7
1.5	Aim and Objective of the Thesis	8
1.6	Organization of the Thesis	9

CHAPTER 2 SHIELDING EFFECTIVENESS

2.1	Introduction	11
2.2	Shielding Effectiveness	11
2.3	SE of Metallic-film Coating on Plastic Substrate	14
2.4	SE of the Array of Dipoles	16
	2.4.1 Reflection Coefficient of the array of dipoles	17

2.5	SE of the Array of Small Square Loops	18
2.5.1	Reflection Coefficient and Absorption Loss of the Array of Dipoles	18

CHAPTER 3 MATHEMATICAL MODELING OF DEVELOPED ANTENNA

3.1	Introduction	20
3.2	V-Conical Antenna	20
3.2.1	Conformal Mapping	22
3.2.2	Antenna Parameters	28
3.2.2.1	Field Patterns	28
3.2.2.2	Directivity	31
3.2.2.3	Gain	33
3.3.	Design Parameters of VCA	33
3.3.1.	Semi-vertical Angle	33
3.3.2.	Azimuth Structural Angle	35
3.4.	Construction of VCA	35
3.4.1.	Fabrication of the Cone	35
3.4.2	Feed Arrangement	36
3.5.	Lens Antenna	37
3.6.	Limitations of the Lens Antenna	38
3.7.	Design Parameters for Lens Antenna	40
3.8.	Construction of Dielectric Lens	42
3.8.1	Selection of Materials	42
3.8.2	Fitting on to VCA	43
3.9	V-Conical Antenna in front of a Lens	44

CHAPTER 4 ANTENNA MEASUREMENT AND SHIELDING

EFFECTIVENESS MEASUREMENT

4.1	Introduction	45
4.2	Test Set Up for Radiation Pattern Measurement	45
4.3	Instrument and other Accessories for Field Measurement	47
4.3.1	Unit Oscillator	47

4.3.2	Spectrum Analyzer	47
4.4	Feed Arrangement	48
4.5	Measurement Procedure	48
4.6	Test result and comparison of antenna parameters with the Theoretical Result	49
4.6.1	Radiation Pattern	49
4.6.2	Gain	55
4.6.3	Directivity	56
4.7.	SE Measurement	56
4.7.1	Test Samples	57
4.7.2	Measurement of SE of the Test Samples	59

CHAPTER 5 CONCLUSION AND RECOMMENDATION OF FUTURE WORK

5.1	Conclusion	62
5.2	Recommendation for future work	63

APPENDICES

Appendix A:	Evaluation of shielding effectiveness of planar sheet	64
Appendix B:	SE of metallic-film coating on plastic substrate	69
Appendix C:	SE of the array of dipoles	72
Appendix D:	SE of the array of small square loops	74

REFERENCES		79
-------------------	--	----

LIST OF ACRONYMS

EMC	Electromagnetic Compatibility
EM	Electromagnetic
EMI	Electromagnetic Interference
EMP	Electromagnetic Pulse
ESD	Electrostatic Discharge
FI	Frequency Independent
SE	Shielding Effectiveness
IL	Insertion Loss
MUT	Material Under Test
N-BNC	N-Type Bayonet Navy Connector
TD	Time Domain
DTC	Dual Transverse Electromagnetic Cell
TEM	Transverse Electromagnetic
RF	Radio Frequency
RFCP	Regularly Filled Conductive Plastic
VCA	V-Conical Antenna
VCLA	V-Conical Lens Antenna

LIST OF SYMBOLS

f	frequency, Hz
ϵ	permittivity, F/m
ϵ_0	permittivity of free space ($= 8.852 \times 10^{-12}$ F/m)
ϵ_r	relative permittivity
μ	permeability, H/m
μ_0	permeability of free space ($= 4\pi \times 10^{-7}$ H/m)
ϕ	azimuth angle, degree
θ_0	semi-vertical angle, degree
λ	wave length, m
λ_0	wave length in free space, m
σ	conductivity
m	meter
ω	angular frequency
\Re	real part
E	electric field
H	magnetic field
D	directivity
U_{av}	average radiation intensity
U_m	maximum radiation intensity
P_r	radiated power, watts
S_r	poynting vector, W/m^2
G	gain
η	radiation efficiency
Z_0	intrinsic impedance of free space ($= 377\Omega$)

LIST OF FIGURES







	Pages
Figure: 1.1(a) Regularly filled conductive plastic sample	03
Figure: 1.1(b) randomly filled conductive plastic sample	03
Figure: 1.1(c) Regularly filled square loop conductive plastic sample	03
Figure: 1.2 Levels of Shielding Effectiveness	03
Figure: 1.3(a) A typical arrangement of measuring the SE of unloaded coupling	04
Figure: 1.3(b) A typical arrangement of measuring the SE of loaded coupling	04
Figure: 1.4 On-line SE measurement during the production cycle	09
Figure: 2.1(a) Reflection of waves at single interface	12
Figure: 2.1(b) Reflection of waves at double interface	12
Figure: 2.2 Array of loaded dipoles in a homogeneous dielectric medium	16
Figure: 2.3 Array of square loops in a homogeneous dielectric medium	19
Figure: 3.1 V-conical lens antenna	21
Figure: 3.2 Conformal mapping for VCA	24
Figure: 3.3 Field pattern of $E_{\theta}(\theta, \phi)$ at $\theta_0=30^{\circ}$ and $\phi_0 = 89^{\circ}$ at the plane $\phi=0$	29
Figure: 3.4 Field pattern of $E_{\theta}(\theta, \phi)$ at $\theta_0=30^{\circ}$ and $\phi_0 = 45^{\circ}$ at the plane $\phi=0$	29
Figure: 3.5 Field pattern of $E_{\theta}(\theta, \phi)$ at $\theta_0=45^{\circ}$ and $\phi_0 = 89^{\circ}$ at the plane $\phi=0$	30
Figure: 3.6 Field pattern of $E_{\theta}(\theta, \phi)$ at $\theta_0=45^{\circ}$ and $\phi_0 = 45^{\circ}$ at the plane $\phi=0$	30
Figure: 3.7 Field pattern of $E_{\phi}(\theta, \pi/2)$ at $\theta_0=45^{\circ}$ and $\phi_0 = 89^{\circ}$ at the plane $\phi = \pi/2$ plane	31
Figure: 3.8 V-Conical Lens Antenna for on-line SE measurement	34

Figure: 3.9	Feed arrangement of VCA	36
Figure: 3.10	Transformation of spherical wave into plane wave while passing through the lens	37
Figure: 3.11	Effect of reflections in the air-lens interfaces.	39
Figure: 3.12	Path lengths in dielectric Lens	40
Figure: 3.13	Geometry of the lens antenna fixed at the face of the a VCLA	41
Figure: 3.14	Constructional details of the dielectric lens.	43
Figure: 3.15	V-Conical lens antenna assembly for on-line SE measurement	44
Figure: 4.1	Field Measurement Set Up.	46
Figure: 4.2	Photograph of the test set up.	46
Figure: 4.3	Feed arrangement with the load connections.	48
Figure: 4.4	Normalized Radiation Pattern at 2m distance ($f = 300$ MHz).	50
Figure: 4.5	Normalized Radiation Pattern at 2m distance ($f = 450$ MHz).	51
Figure: 4.6	Normalized Radiation Pattern at 3m distance ($f = 300$ MHz).	52
Figure: 4.7	Normalized Radiation Pattern at 3m distance ($f = 450$ MHz).	53
Figure: 4.8	Normalized Radiation Pattern at 3m distance ($f = 600$ MHz).	54
Figure: 4.9	Comparison of Gain vs. Frequency at 3m distance.	56
Figure: 4.10	Photograph of test samples	58
Figure: 4.11	Measurement of signal strength without MUT.	59
Figure: 4.12	Measurement of signal strength with MUT.	60
Figure: 4.13	Variation of SE values of different types of conductive plastics.	60
Figure: 4.14	Comparison of SE of a aluminium sheet between measured SE values and theoretically calculated SE values.	61
Figure: 4.15	Comparison of SE values of a aluminium foil between Measured values and theoretically computed values.	61

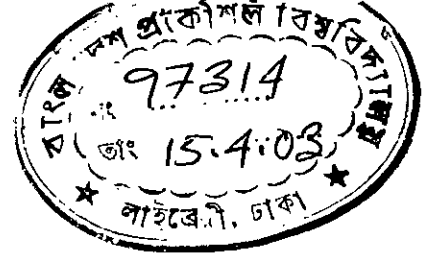


CHAPTER 1

ELECTROMAGNETIC COMPATIBILITY

-  **INTRODUCTION**
-  **SHIELDING MATERIALS**
-  **MEASUREMENT OF SHIELDING EFFECTIVENESS**
-  **BENEFITS OF ON-LINE SE MEASUREMENT**
-  **AIM AND OBJECTIVE OF THE THESIS**
-  **ORGANIZATION OF THE THESIS**

CHAPTER- 1



ELECTROMAGNETIC COMPATIBILITY

1.1 INTRODUCTION

Electromagnetic Compatibility (EMC) is the capability of electronic equipment or systems to be operated in the intended operational electromagnetic environment. Because of the widespread proliferation of electronic appliance, the emergence of microprocessor, micro-controllers, and miniaturization of computers along with the development of Satellite Communication, EMC has gained paramount importance. The EMC studies both reflect and promote the awareness among the designers and manufacturers of electronic equipment of the need to combat Electromagnetic Interference (EMI) from both inter- and intra - devices.

The EMI from a equipment can be controlled or minimized by enclosing the equipment with a conductive-shielded enclosure. Conductive composite plastic material is now being widely used for the shielded enclosure to reduce ingress or emission of electromagnetic of electromagnetic interference problem of the equipment [1] - [3]. Two types of conductive composite are found such as surface metallized plastic and filled composite plastic. Filled composite is now widely used in the electronic industry to combat against EMI as well as for electrostatic discharge (ESD).

The level of shielding against EMI is usually determined by the Shielding Effectiveness (SE) of the material used for the enclosure [4]. The term SE is defined as the ratio of the magnitude of the EM field that is incident on the shield of the magnitude of the EM field that is transmitted through the shield. In this work an EMC antenna is proposed for measurement of SE for plane wave plane wave.

In this chapter different types of material used for EMC shielding is briefly described in section 1.2. A comprehensive review of different techniques used for measuring the shielding effectiveness is presented in section 1.3. Benefits of on-line SE measurement are given in section 1.4. Section 1.5 contains the aim and objectives of this thesis. Organization of the thesis is given in section 1.6.

1.2 SHIELDING MATERIALS

A good quality shielding material is one of the prime factor to reduce EMI. Plastic materials which are commonly used as the polymeric resins are polycarbonate, acrylonitrile butadiene styrene (ABS), polystyrene, nylon, polyphenylene oxide, polyethylene, polypropylene and maleated polystyrene (SMA) co-polymer. A number of techniques are available to impart conductivity in this plastics. The following are the various techniques for metallizing plastic for EM shielding materials.

Surface Metallized Plastic where the inner surface of the plastic is coated with a metallic coating. The SE values of this type of material depends on the type of conductive filler and paint thickness.

Flexible Laminates of metal foil (usually aluminium and copper) bonded to a reinforcing substrate (e.g. polyester, PVC, polyamide etc.) are used as shielding material [5]. The SE of such materials essentially depends on the thickness and conductivity of the metal foil used.

Conductive Fabrics are fine wires of solid metals (e.g. nickel, copper, silver and gold) woven, knitted or formed into sheets to be glued with fabrics (e.g. polyester, polyamide, rayon). Conductive fabrics can be used for imparting shielding capability to plastics in lieu of conductive paint or other metallic coating [6].

Filled Composite Plastic is a homogeneous mixture of plastic resin and conductive filler, usually metal or carbon. The most widely used conductive fillers in the form of flake or

fibre are graphite, copper, aluminium, stainless steel, nickel and nickel coated carbon. SE depends on the type and amount of conductive filler added to the plastic. Filler in the plastic may be arranged either in the regular form or in random form or in regular square loop as shown in Fig.1.1 (a), Fig.1.1 (b) and Fig.1.1 (c) respectively. Filled composites are widely used in electronic industry for electrostatic discharge (ESD) protection in silicon chip storage bins, anti static floor mats, handling gloves and wrist straps which ground any build up of static electricity. This can be used for shielding of personal computer, signal generator, vacuum tube etc.

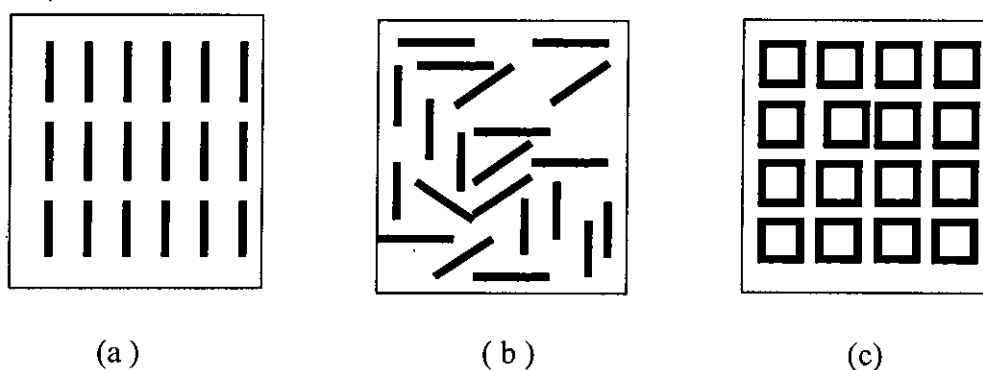


Fig.1.1 Filled conductive plastic samples (a) Regularly filled conductive plastic (b) Randomly filled conductive plastic and (c) Regularly filled square loop conductive plastic.

The level of shielding effectiveness of a material is given in Fig 1.2.

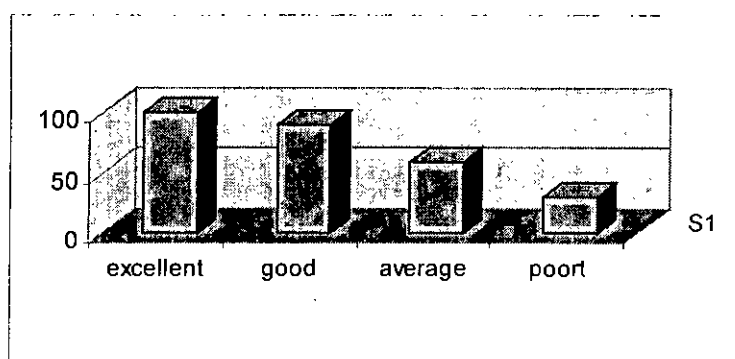


Fig1.2 Levels of Shielding Effectiveness.

1.3 MEASUREMENT OF SHIELDING EFFECTIVENESS:

Generally SE measurement technique is referred to as insertion loss (IL) that results from introducing the test sample. A diagram for IL measurement is shown in Fig.1.3. IL is measured by comparing the received signal strength with the MUT (P_R) and without the MUT (P_R) in the test device with keeping the transmitted power (P_T) constant. This can be written as [7].

$$IL = 10 \log_{10}(P_R/P_R') \quad (1.1)$$

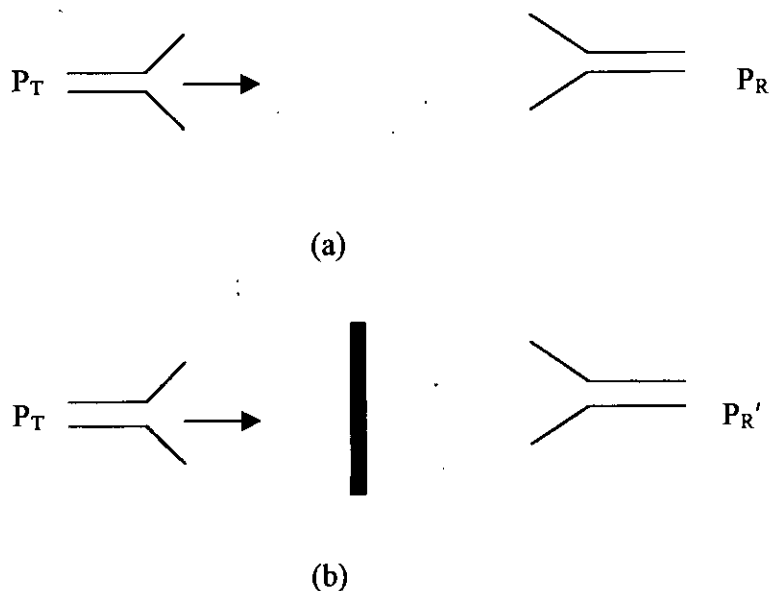


Fig.1.3. A typical arrangement for measuring the SE of material.(a) unloaded coupling (b) loaded coupling.

Commonly used shielding effectiveness measurement technique is MIL-STD-285 [8]. In this method the MUT is mounted over an aperture in the wall of a shielded room. The transmission loss can then be measured by placing two antennas, one inside the shielded room and the other outside the shielded room. Then it will be compared with the transmission loss between the same two antennas at the same separation in free space. This method is simple, but time consuming and lacks of repeatability.

In Circular Co-axial Transmission Line Holders SE can be measured in two ways. These are (a) Continuous Conductor (CC) and (b) Split Conductor (SC) version.

In Continuous Conductor(CC) version the test device is a section of expanded 50Ω co-axial line. The holder may be disassembled to allow the insertion of an annular washer shaped test sample. When assembled both the inner and outer conductor, it ideally forms continuous connections. The CC holder is quite easy to use and lends itself well to an automated system.

In Split Conductor Version the inner conductor is not continuous, it is also segmented in two parts. The sample shape is no longer annular. Two pieces of material are needed as sample. Measurement for the loaded case require a disk shaped sample with diameter equal to that of the outer flange dimension. The unloaded reference measurement is done with an annular piece of material matching the outer flange dimensions and a disk matching the diameter of the inner conductor. This is comparatively complicated method.

In Time Domain Approach instead of continuous wave sources, pulsed or time domain (TD) signals are directed through the test sample. Use of a TD source makes it possible to differentiate between the direct path and indirect path, signal at the receiving end. An impulse generator is used to generate an impulse of a few hundreds of pico-second width to be radiated through a TEM horn antenna. At the receiving end the pulse is detected by a similar antenna connected to a waveform recorder. The transmitting antenna is spaced sufficiently from the test material so that it is in the far field region of the sample. Ideally a large sample sheet is required with this method. The time domain approach is fast, broad-band, and compatible with other plane wave simulation techniques, especially when a large sheet of sample is available. In this method initial higher cost is involved to prepare the test set up.

In Complex Permittivity Approach the complex permittivity of the dielectric material is measured by a open-ended co-axial probe. The SE value of the material is then calculated

from the complex permittivity. A new and simple technique for measuring the complex permittivity of planar sheet like materials has been proposed by Scott [9], where the MUT is sandwiched between a pair of open-ended flanged coaxial probes. No sample preparation is necessary which is an obvious advantage of this technique in the control of on-line SE determination. But it is an indirect method for SE measurement.

TEM Cell is an expanded section of a rectangular co-axial transmission line. In Dual TEM Cell (DTC) two identical TEM cells are connected in piggy-back style. A common aperture used in DTC test fixture. An aperture is cut in the top wall of the cell's outer conductor. Then a known and uniform field is generated in the cell would couple through the aperture. Then another cell is placed on top of the first one in piggy-back style. In this way, the field radiated in the first cell can be measured in the second cell. The MUT is placed over the aperture. It is seen that the coupling from the source cell to the sensor cell is reduced. The amount of this reduction is a direct measure of the materials IL. It has two output parts for a given input signal. The coupling through the aperture in the forward direction of the receiving cell is proportional to the difference of the normal electric and tangential magnetic polarizabilities of the aperture while that in the backward direction is proportional to the sum of the polarizabilities [10]. Thus by hybridizing the two output ports for summing and subtracting, one low impedance near field situations individually. This method is suitable for near field (E-field) SE measurement.

TEM-T Cell SE measurement technique has been reported by Hariya [11] and Catrysse[12]. The TEM cell almost resemble a flanged co-axial holder except that the cross-section is rectangular like TEM cell. Magnetic field SE and electric field SE are measured separately in two different test devices. The sample must be covered the outer flanges but the center conductor should not touch the sample because the coupling between this conductor and the sample is capacitive in nature.

The concept of Surface Transfer Impedance [13] constitutes a basis for calculating SE of samples having specific geometric shape. For a locally planar shield, the approximate expression for the SE is given by [14].

$$SE = 20 \log_{10} \left| \frac{Z}{Z_{st}} \right| \quad (1.2)$$

Where, Z_{st} =The surface transfer impedance

Z =An impedance term which is a function of the incident field type and the shield geometry.

A coaxial test fixture is used for measuring the transfer impedance. The fixture allows pressurized air to be injected into the top chamber, enabling accurate, uniform control of the pressure exerted on the test sample. Very good electrical contact can thus be ensured. The coaxial structure makes it easy to determine the frequency dependence of the transfer impedance.

A general description of EMC measurements has been given and the variables of interest of the SE measurement systems are noted. Moreover existing SE measurement techniques have been reviewed. All the reviewed techniques are suitable for off-line SE measurement which is time consumable and cost involvement is high. In this work on-line SE is measured by using an EMC antenna namely, V-Conical Lens Antenna (VCLA) in order to overcome those limitations.

1.4 BENEFITS OF ON-LINE SE MEASUREMENT

Like other on-line product characterization, SE measurements of planar sheet during production cycle may also play a very important role in the manufacturing process. Determination of insertion loss or SE of planar sheet during production cycle is important for waste reduction, quality control and possible improvement of SE. A number of techniques are available to measure off-line SE of this material. In all cases the sample preparation is necessary. In on-line SE measurement, the mechanism of imparting shielding capability to the material may be regulated accordingly. This would in turn ensure waste reduction. Off-line SE measurement incurs costly spoilage of materials, thereby increase the overall production cost. Another important feature of on-line SE

measurement is the significant reduction in time, time of the manufacturing process and personnel. Off-line measurement increases the production cost. On-line SE measurement may be a very efficient inclusion in the production cycle of the newly proposed RFCP (Regularly Filled Conductive Plastic) type of filled composites.

1.5 AIM AND OBJECTIVE OF THE THESIS

There are of course a lot of techniques available for assessing the shielding capability of conductive plastics but are mostly for laboratory measurements. That is why these methods are unsuitable for on-line SE measurement. Determination of SE of planar sheet during production cycle is important for waste reduction, quality control and possible improvement of SE which is shown by a simple Fig.1.4.

This research work, therefore is aimed at designing and developing an EMC antenna for on-line plane wave SE measurement of different types of planar sheet. To achieve this aim the following objectives were envisaged.

- Development of mathematical model of the V-Conical Antenna in front of a lens by using conformal mapping.
- Design and construction of V-Conical antenna and a plano-convex dielectric lens which is made of polyamide-nylon by using Fermat's principle. Then these are assembled together in order to construct V-Conical Lens Antenna (VCLA).
- Computation of the antenna parameters such as field patterns, directivity, gain etc.
- Comparison of the developed antenna parameters with the theoretically computed values.

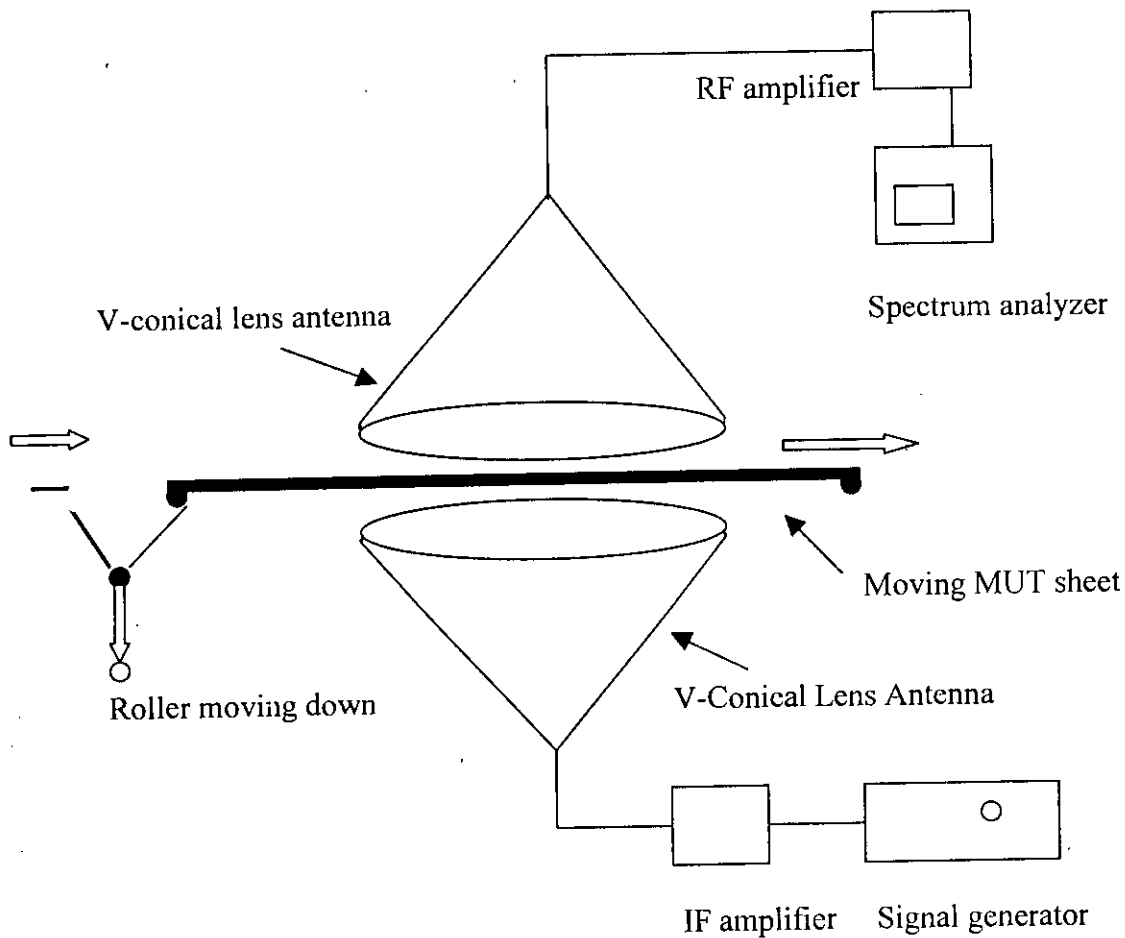


Fig.1.4 On-line SE measurement during the production cycle.

1.6 ORGANIZATION OF THE THESIS

The thesis is organized as follow






Theoretical analysis of shielding effectiveness measurement for various type of materials is given chapter 2. Electromagnetic field solution by conformal mapping antenna parameters such as directivity, gain, and field patterns for VCA are discussed in chapter 3. Chapter 3 also contains an elaborate description of the design and construction of V-Conical Lens Antenna. Antenna measurement and shielding effectiveness measurement are described in chapter 4. Chapter 4 also contains SE measurement procedure of different kind of materials, a comparative study of results between measured results and

theoretical results. The conclusion and recommendations for the further research are given in chapter 5.



CHAPTER 2

SHIELDING EFFECTIVENESS

-  INTRODUCTION
-  SHIELDING EFFECTIVENESS
-  SE OF METALLIC-FILM COATING ON PLASTIC SUBSTRATE
-  SE OF THE ARRAY OF DIPOLES
-  SE OF THE ARRAY OF SMALL SQUARE LOOPS

CHAPTER –2

SHIELDING EFFECTIVENESS

2.1 INTRODUCTION

SE measurement is crucial in determining the EMC of an item of equipment. The objective of this work is to develop SE measurement techniques to determine the shielding capability of conductive composite materials during their production process where the material under test (MUT) would most often be in sheet form. Now a days various types of materials are used to determine SE of a material which are discussed in previous chapter. The SE of such materials essentially depends on thickness, conductivity, type and amount of conductive filler added to the plastic substrate.

Shielding effectiveness of sheet like materials is stated in section 2.2. In section 2.3 determination of SE of metallic-film coating on plastic substrate has been given. SE and reflection coefficient of the array of dipoles have been discussed in section 2.4. In section 2.5 SE, reflection coefficient and absorption loss of the array of small square loops are given section 2.5.

2.2 SHIELDING EFFECTIVENESS

Shielding effectiveness or insertion loss, representing the reduction (expressed in dB) of the level of an electromagnetic wave at a point in space after a metallic barrier is inserted between that point and the source. More precisely, SE refers to the ability of a material to guard against EMI both against emission and susceptibility. SE of a material can also be expressed as

$$SE = A + R + C \quad \text{dB} \quad (2.1)$$

where

- A → Absorption loss
- R → Reflection loss
- C → Correction term

The reflection loss expression is given on the basis that the reflected wave either travels back to infinity or suffers sufficiently high penetration loss that successive re-reflections may be neglected as in Fig.2.1(a) and Fig.2.1 (b) respectively.

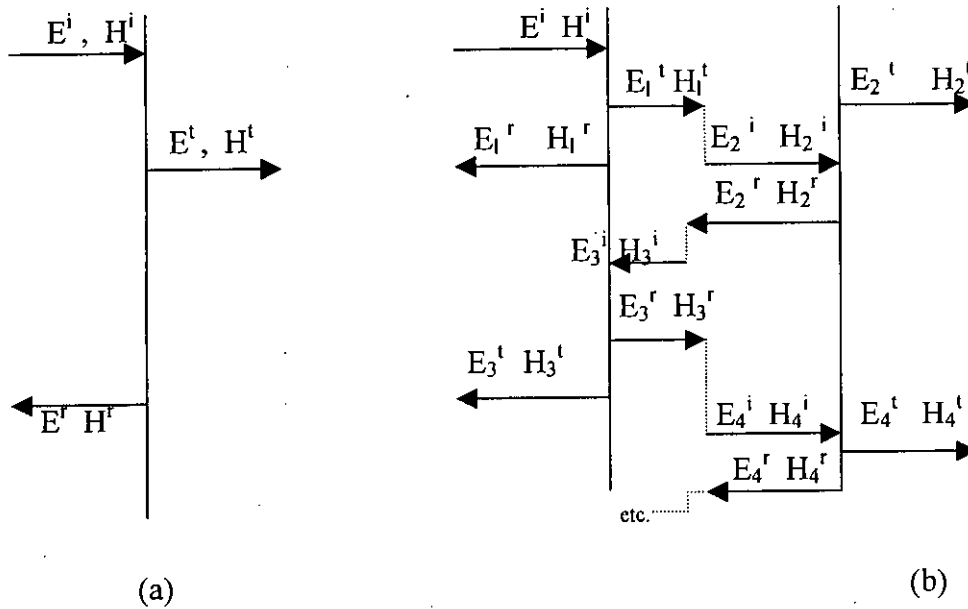


Fig.2.1 Reflection of waves at interfaces. (a) Single interface. (b) Double interface (single shield) showing multiple re-reflections [1].

The Shielding Effectiveness may be evaluated from well-known two-wire transmission line equations [1] which is given in appendix-A. The reflection loss can be written in terms of transmission coefficient for a infinite planar sheet of thickness l as

$$R = -20 \log_{10} |p| = 20 \log_{10} \frac{|1 + k|^2}{4|k|} \quad (2.2)$$

Where

$$k = Z(l)/\eta$$

$Z(l)$ is the impedance looking to the right of the plane $x = l$.

η is the intrinsic impedance of the sheet materials.

The reflection loss expressed in Equ.(2.2) is on the basis that the reflected wave travels back to infinity or suffers sufficiently high penetration loss that successive re-reflections may be neglected as in Fig.2.1(a).

Fig.2.1(b) is the more general case whereby successive re-reflections may not be neglected. For this case, the total shielding effectiveness, which is evaluated in appendix-1 can be written as

$$S = -20 \log_{10} |T| \quad (2.3)$$

$$= 20 \log_{10} \left| \frac{(1 - qe^{-2\gamma t})e^{\gamma t}}{p} \right|$$

$$= 20 \log_{10} |e^{\gamma t}| - 20 \log_{10} |p| + 20 \log_{10} |1 - qe^{-2\gamma t}| \quad (2.4)$$

Where,

p is the transmission coefficient

q is the reflection coefficient

γ is the propagation constant

Expression (2.4) is the complete formula for shielding effectiveness of a single shield where the first term represents the absorption loss, the second term represents the reflection loss and the third term represents the correction term for successive reflections.

For a metallic sheet of thickness t the absorption loss and reflection loss further can be written as [15]:

$$A = 8.686 \alpha t \sqrt{(\pi \mu \sigma)} \quad (2.5)$$

and

$$R = 20 \log_{10} \frac{|1 + k|^2}{4|k|} \quad (2.6)$$

The positive or negative correction term which need not be taken into account when A is more than 15dB. It is caused by the reflecting waves inside the shielding barrier and is calculated in dB. When a metallic barrier has an absorption loss (A) of less than 15 dB, it is designed as “electrically thin”.

2.3 SE OF METALLIC- FILM COATING ON PLASTIC SUBSTRATE

A conductor of high conductivity and low permeability has low intrinsic impedance. When a radio wave propagates from a medium of high intrinsic impedance into a medium of low intrinsic impedance, the reflection coefficient is high. From electromagnetic plane wave theory in the far field, high attenuation occurs in a medium made of material having high conductivity and low permeability. Good conductors, such as gold, silver, copper, aluminium, have high conductivity and are often used as the material for attenuating electromagnetic energy. Microwave radiation attenuation by a metallic film coating on substrate consists of three parts such as absorption loss, reflection loss and successive re-reflection loss [15]. Details of these are given in Appendix-B.

If the plastic substrate is assumed to be a non-absorbing material, the absorption loss (A) of the metallic-film coating on a substrate is related to the thickness t of the coated film as shown:

$$A=8.686t\sqrt{(\pi f\mu\sigma_f)} \quad \text{dB} \quad (2.7)$$

where,

t = thickness of the film coating in meter

μ = permeability of the film in henrys per meter

f = frequency in hertz

σ_f = conductivity of the coated film in mhos per meter

Since the thickness of the coated film is very thin, the absorption loss A is very small and can be ignored.

The reflection loss (R) due to the multiple boundaries of the substrate glass coated with a metallic film can be expressed as [15]

$$R \approx 20 \log \left[28.33 \sqrt{\frac{\sigma_f}{\mu f}} \right] = 88 + 10 \log \left(\frac{\sigma_f}{f} \right) \quad \text{dB} \quad (2.8)$$

The successive re-reflection loss (C) is given by [16]

$$C = 20 \log | 1 - \rho 10^{-A/10} (\cos \theta - j \sin \theta) | \quad (2.9)$$

Where

$$\rho = \left(\frac{\eta_f - \eta_a}{\eta_f + \eta_a} \right)^2 \approx 1 \quad \text{for} \quad \eta_a \gg \eta_f$$

$$\theta = 3.5 t \sqrt{f \mu \sigma_f}$$

The above equation is valid when the absorption loss is much less than 10 dB, i.e. for electrically thin film coated material. Over the frequency range of 100 MHz to 40GHz, the angle θ is much smaller than 1° so that $\cos \theta \approx 1$ and $\sin \theta \approx \theta$. Thus the correction term of Eqn. (2.9) can be simplified to

$$C \approx 20 \log [3.5 t \sqrt{f \mu \sigma_f}] = -48 + 20 \log [t \sqrt{f \sigma_f}] \quad \text{dB} \quad (2.10)$$

Finally, the total microwave radiation attenuation by a metallic coating on a glass substrate for plane wave, becomes as

$$\text{Attenuation} = 40 - 20 \log_{10}(R_s) \quad (2.11)$$

Where $R_s = 1/t\sigma_f$ Ω/square

It is interesting to note that the microwave radiation attenuation due to the coated metallic film on a substrate in the far field is independent of frequency and is related only to the surface resistance of the coated metallic film.

2.4 SE OF THE ARRAY OF DIPOLES

SE consists of absorption loss (A), reflection loss (R) and successive re-reflection loss (B) of the RFCP. For a doubly periodic array of dipoles in an equivalent homogeneous medium (ϵ_{re}) as shown in Fig.2.2, there will be no absorption loss due to the use of strip like filler. Successive reflection loss is very negligible. SE of the array of dipoles [Appendix-C] in a homogeneous medium having an effective dielectric constant (ϵ_{re}) can then be expressed as follow

$$SE = R \quad \text{dB} \quad (2.12)$$

Reflection loss (R) can be determined by multiplying the incident power with the reflection coefficient (R'):

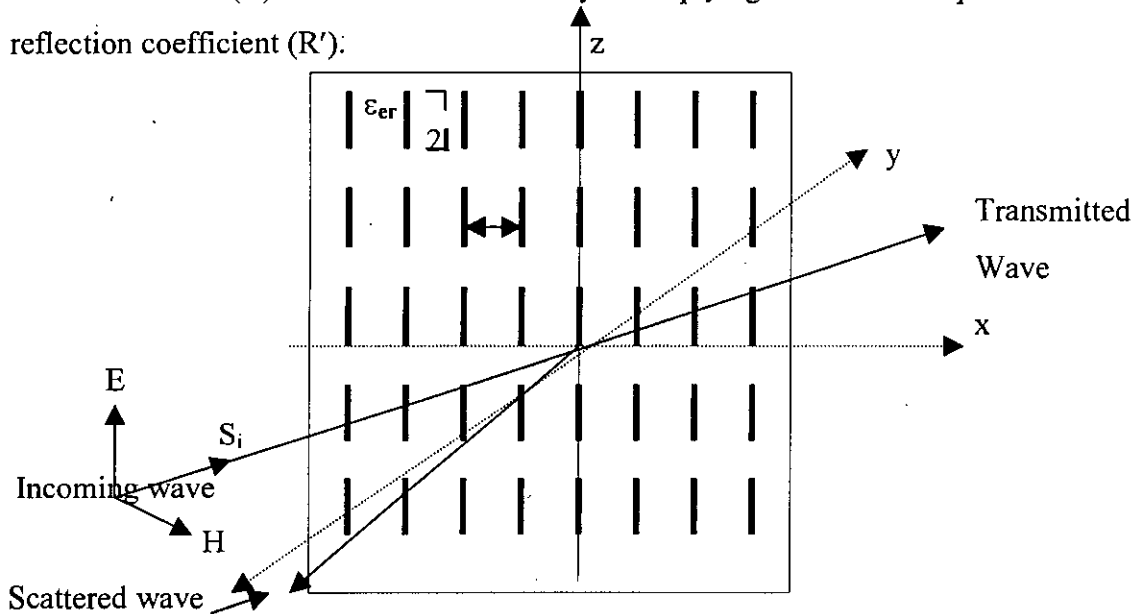


Fig.2.2 Array of loaded dipoles in a homogeneous dielectric medium (ϵ_{er}) and incident EM wave with vertical polarization.

2.4.1 Reflection coefficient of the array of dipoles

A plane wave, which is incident on the periodic array of dipoles as shown in Fig. 2.2 is considered to be linearly polarized in z direction. The direction of propagation lies in the x-y plane, making an angle ϕ_1 with negative y-axis as shown in Fig2.2. The specular reflection for such an array can be expressed as [17].

$$R' = \frac{K(l_\lambda, l_e, Z_L, Z_A) l^4 \sec^2 \phi_i}{[D_x D_z (Z_A + Z_L)]^2} \quad (2.13)$$

Where

$$K(l_\lambda, l_e, Z_L, Z_A) = 3600 \frac{\left| F_{e1} - \left(\frac{Z_L}{Z_A} \right) F_{e2} \right|^2 F_{e3}^2}{\pi^2 l_\lambda^4}$$

$$F_{e1} = \frac{\sin \beta l - \beta l_e \cos \beta l_e}{1 - \cos \beta l_e}$$

$$F_{e2} = \frac{1}{\sin \beta l_e} [1 - \cos \beta l_e - F_{e1} \sin \beta l_e]$$

$$F_{e3} = \frac{\cos \beta \Delta l - \cos \beta l_e}{\sin \beta l_e}$$

In above equations, $l_\lambda = l/\lambda$

where λ is the wave length of the incident wave, $\Delta l = l_e - l$,

$\beta = 2\pi/\lambda$ is the phase constant

Z_A is the driving point impedance of each element and

Z_L is the impedance loaded in each dipole

D_x is the distance between two identical elements

D_z is the distance between two adjacent rows

l and l_e is the half of the length of element and effective length of the element respectively.

The driving point impedance of the array can be written as [17].

$$Z_A = \sum_{r'=-R'}^{R'} \sum_{k=-K}^K \epsilon_k Z_{r',k} \cos(\beta D_x k \sin \phi_i) \quad (2.14)$$

where ϵ_k is the Neumann factor defined by

$$\begin{aligned} \epsilon_k &= 1 \quad \text{for } k = 0 \\ &= 2 \quad \text{for } k \neq 0 \end{aligned}$$

2.5 SE OF THE ARRAY OF SMALL SQUARE LOOPS

For the array of small square loops in a homogeneous medium having an effective dielectric constant (ϵ_{er}), reflection loss (R) as well as absorption loss (A) will be available. There will be no successive reflection loss (B) due to the use of thin square loop like filler. Evaluation of SE of such RFCP is given in Appendix-D can be expressed as

$$SE = A + R \quad \text{dB} \quad (2.15)$$

Where A is the absorption loss and
 R is the reflection loss.

Reflection coefficient and absorption loss are discussed in following subsections.

2.5.1 Reflection coefficient and absorption loss of the array of small square loops

A doubly periodic array of small square loops in a homogeneous medium having an effective dielectric constant (ϵ_{er}) is shown in Fig.2.3. In this case for computing the reflection coefficient, this type of array configuration has been considered as a combination of vertical (z-directed) array and horizontal (x-directed) array of dipoles by satisfying the following conditions [18].

- number of rows and number of columns of the vertical and horizontal dipole array must be even and equal i. e. $r_1' = r_2'' = r'$ and $k_1 = k_2 = k$.
- length of element for both the vertical and horizontal arrays must be equal and should be electrically small.

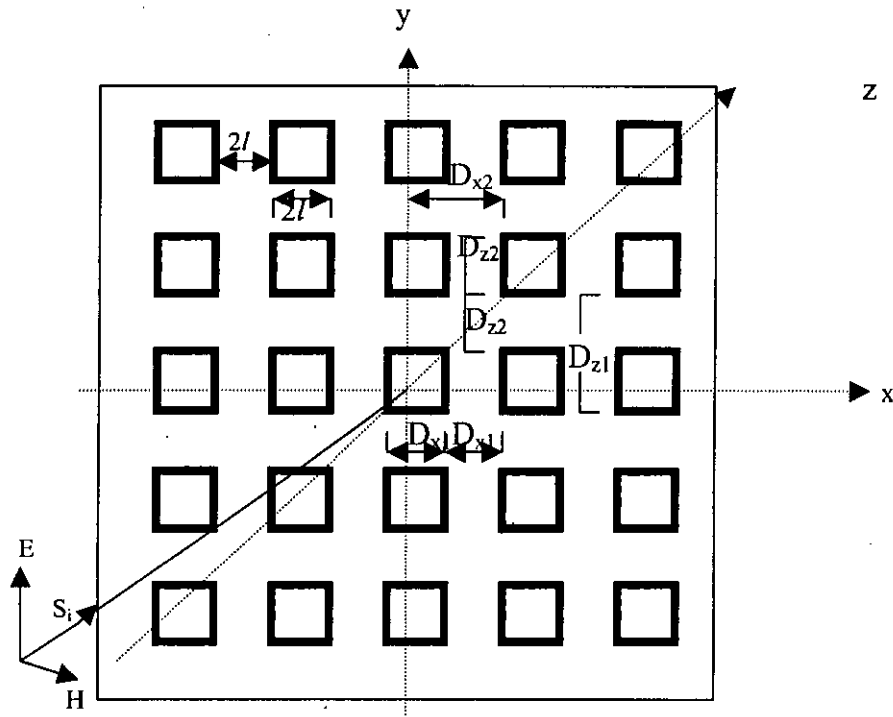


Fig 2.3 :Array of square loops in a homogeneous dielectric medium (ϵ_{er}).

- spacing between two adjacent array elements in the case of vertical array (i. e. z-directed) will be as follow: $D_{x2} = 2l$ and $D_{z2} = 2D_{z1} = 4l$
- spacing between two adjacent array element in the case of horizontal array (x-directed) will be as follow: $D_{x2} = 2D_{x1} = 4l$ and $D_{z2} = 2l$

The reflection coefficient of the array of small square loops as shown in Fig.2.3 will then be

$$R' = R'_1 + R'_2 \quad (2.16)$$

Where, R'_1 is the reflection coefficient of the vertical array of dipoles and R'_2 is the reflection coefficient of the horizontal array of dipoles. Absorption loss of the array of small square loops can be expressed as (Appendix- D):

$$A = 10\log_{10}(A_L M) \quad \text{dB} \quad (2.17)$$

Where M is the total number of loops in the array.



CHAPTER 3

MATHEMATICAL MODELING OF DEVELOPED ANTENNA

 **INTRODUCTION**

 **V-CONICAL ANTENNA**

 **DESIGN PARAMETERS OF VCA**

 **CONSTRUCTION OF VCA**

 **LENS ANTENNA**

 **LIMITATIONS OF THE LENS ANTENNA**

 **DESIGN PARAMETERS FOR LENS ANTENNA**

 **CONSTRUCTION OF DIELECTRIC LENS**

 **V-CONICAL ANTENNA IN FRONT OF A LENS**

CHAPTER - 3

MATHEMATICAL MODELING OF DEVELOPED ANTENNA

3.1 INTRODUCTION

The VCA is a Frequency Independent (FI) antenna and this type of antenna has no theoretical limitation on the bandwidth of operation [3]. It was first observed by Sumsey with Mushiake's in 1949 that self complimentary antennas have a constant impedance or half the intrinsic impedance of space, at all frequencies and organized a principle that "the impedance and pattern properties of an antenna will be frequency independent if the antenna shape is specified only in terms of angles". Practically, however, the performance cannot be even approximately constant for all frequencies. The VCA is an angular antenna and the electromagnetic fields are pure spherical waves of transverse electromagnetic (TEM)-mode even in the near region [19]. An EMC antenna namely VCA in front of a lens is designed and developed in which the lens fitted to its (V-Cone's) open mouth, transforms this spherical wave into a uniform plane wave and the combination thus simulates a standard far field situation. In the section 3.2 the analytical model of the field distribution and antenna parameters in front of such an assembly is presented by conformal mapping. Design parameters and construction of VCA is discussed in the section 3.3. and 3.4 respectively. In section 3.5 lens antenna is presented. Limitations and design parameters of lens antenna have been described in section 3.6 and 3.7 respectively. Construction of dielectric lens is described in section 3.8. V-Conical Antenna in front of a lens is presented in section 3.9.

3.2 V-CONICAL ANTENNA

Normally any infinitely long bi-conical (angular) antenna is characterized by FI when the point source is located at the origin of the co-ordinates [19]. It is an ideal pulse antenna. As shown in Fig.3.1.the angular antenna has the metal surfaces that are functions of

angular coordinates rather than the radial coordinate r . When the driving voltage is applied at the origin O the currents and charges on the surfaces and the electromagnetic fields in space are all spherical waves of the form

$$f(\theta, \phi) \frac{e^{-jkr}}{r}$$

Where, $f(\theta, \phi)$ is the directional distribution determined by the angular structure of the antenna and that why this is frequency independent. In the case of pulse operation, where one can use tapered resistive termination to eliminate the reflected pulses, such bi-conical antennas have been widely used in radiative electromagnetic pulse (EMP) simulators or other pulse launchers. However, due to the fact that the azimuth directivity is uniform the energy efficiency could be improved by incorporating some directionality in the simulator design. The VCA, as shown in fig.3.1 is a pair of long arc shaped metal plates, each of them bent around a cone or a V linear antenna rotated at an angle $2\phi_0$. The construction of VCA depends only two angles; the semi-vertical angle θ_0 and the azimuth angle ϕ_0 . When the source is located at the origin O , and the boundaries are

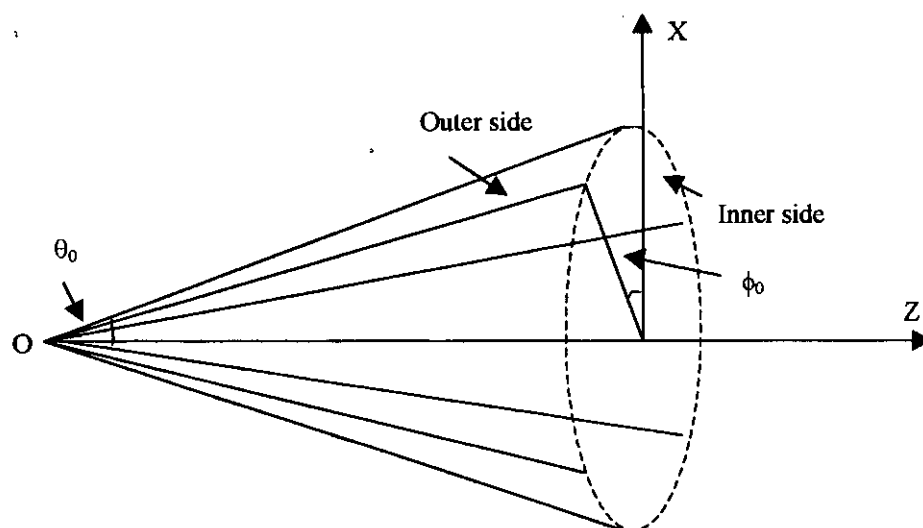


Fig 3.1 V-Conical Antenna.

related to angular dimensions, it has been proved that the excited electromagnetic wave is in the TEM-mode only [20]. The electromagnetic field in free space can be expressed in terms of Hertz Scalar functions, Π_{er} .

$$E_r = 0 \qquad H_r = 0 \qquad (3.1)$$

$$E_\theta = \frac{1}{r} \frac{\partial^2 \Pi_{er}}{\partial r \partial \theta} \qquad H_\theta = \frac{j\omega\epsilon}{r \sin \theta} \frac{\partial \Pi_{er}}{\partial \phi} \qquad (3.2)$$

$$E_\phi = \frac{1}{r \sin \theta} \frac{\partial^2 \Pi_{er}}{\partial r \partial \phi} \qquad H_\phi = -\frac{j\omega\epsilon}{r} \frac{\partial \Pi_{er}}{\partial \theta} \qquad (3.3)$$

Where $\Pi_{er} = \Pi(\theta, \phi)e^{-jk_r r}$ satisfies the Helmholtz equation

$$(\nabla^2 + k^2) \frac{\Pi_{er}}{r} = 0$$

and $\Pi_{er}(\theta, \phi)$ satisfies the equation

$$\left[\sin \theta \frac{\partial}{\partial \theta} \left(\sin \theta \frac{\partial}{\partial \theta} \right) + \frac{\partial^2}{\partial \phi^2} \right] \Pi(\theta, \phi) = 0 \qquad (3.4)$$

The boundary condition for $\Pi(\theta, \phi)$ can be obtained from the excitation condition

$$\frac{V_0}{2} = \lim_{r \rightarrow 0} \int_0^{\theta_0} -E_\theta r d\theta \qquad (3.5)$$

The substitution of Eqn.(3.3) into Eqn.(3.5) leads to the boundary condition for $\Pi(\theta, \phi)$:

$$\Pi(\theta, \phi) = -\frac{jV_0}{2k}, \quad |\phi| < \phi_0, \qquad (3.6)$$

and

$$\Pi(\theta, \phi) = \frac{jV_0}{2k}, \quad |\pi - \phi| < \phi_0, \theta = \theta_0. \qquad (3.7)$$

3.2.1 Conformal Mapping

The boundary value problem Eqn.(3.5) and Eqn.(3.7), can be solved by conformal mapping. Let $\rho=\tan(\theta/2)$ and $\rho_0=\tan(\theta_0/2)$. Then Eqn.(3.5) becomes

$$\left(\rho \frac{\partial}{\partial \rho} \rho \frac{\partial}{\partial \rho} + \frac{\partial^2}{\partial \phi^2}\right) \Pi = 0 \quad (3.8)$$

or

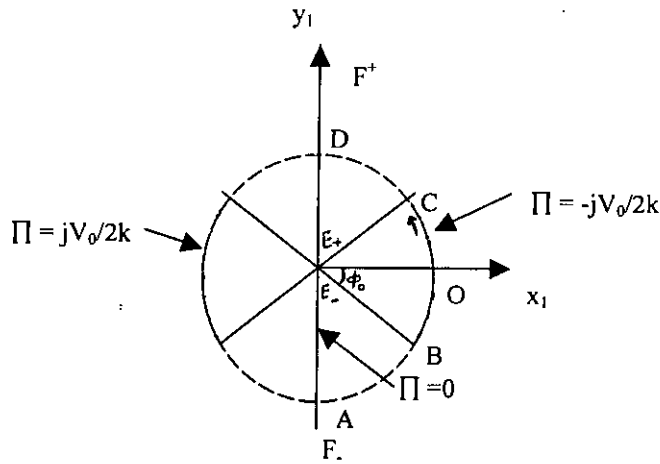
$$\left(\frac{\partial^2}{\partial x_1^2} + \frac{\partial^2}{\partial y_1^2}\right) \Pi = 0 \quad (3.9)$$

where $x_1=\rho\cos\phi$, $y_1=\rho\sin\phi$ and $z_1=x_1+j y_1$.

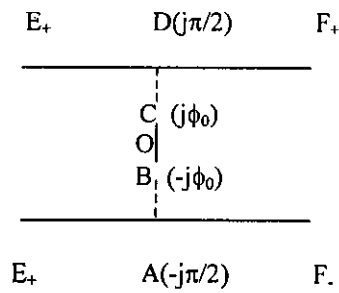
This is a two-dimensional Laplace equation. The boundaries in the new z_1 plane are shown in Fig 3.2(a). The problem now becomes a static electric problem, i.e., a potential difference across symmetrical circular electrodes. This problem can be solved by the following conformal mapping.

Due to the geometrical symmetry, the y_1 axis is a zero-potential line and only half of the z_1 plane needs to be analyzed. The transformation $z_2 = x_2 + jy_2 = \ln(z_1/\rho_0) = \ln(\rho/\rho_0) + j\phi$ maps the right of the z_1 plane into a strip in the z_2 as shown in Fig 3.2(b) where corresponding points in the two planes are denoted by the same letters and the left side of the strip corresponds to the area inside the half circle of radius ρ_0 on the right in the z_1 plane. Due to the electrical and geometrical symmetry in the z_2 plane, it is obvious that the straight dotted lines BA and CD should be the lines of the electric force. The transformation $z_3 = x_3 + jy_3 = \sin(jz_2)$ maps the left side of the strip in the z_2 plane into the lower z_3 plane where the equipotential lines BC and AED and the lines of force BS and CD are all along the real x_3 axis, as shown in Fig3.2(c). With the Schwarz-Christoffel transformation z_4 can be written as

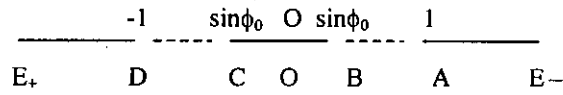
$$\begin{aligned} z_4 = x_4 + jy_4 &= \int_0^{z_3} \frac{dx}{\sqrt{(x^2 - 1)(x^2 - \sin^2 \phi_0)}} \\ &= \int_0^{jz_2} \frac{d\alpha}{\sqrt{\sin^2 \phi_0 - \sin^2 \alpha}} \end{aligned} \quad (3.10)$$



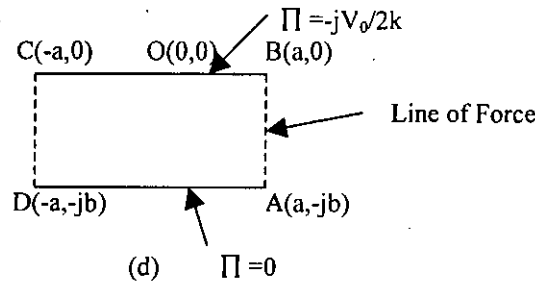
(a)



(b)



(c)



(d)

Fig.3.2 Conformal mapping for VCA. (a) Equivalent static problem, z_1 plane; $z_1 = \rho e^{j\phi} = \tan(\theta/2)e^{j\phi}$. (b) z_2 plane; $z_2 = \ln(z_1/\rho_0)$. (c) z_3 plane; $z_3 = \sin(jz_2)$. (d) z_4 plane; $z_4 = \int_0^{z_3} \frac{z^3}{(x^2-1)(x^2-\sin^2\phi_0)} dx$.

the lower z_3 plane is mapped into a rectangle in the z_4 plane, where the two sides (2a,b) of the rectangle are {Fig 3.2(d)}

$$\begin{aligned}
 a &= \int_0^{\phi_0} \frac{d\alpha}{\sqrt{\sin^2 \phi_0 - \sin^2 \alpha}} \\
 &= \int_0^{\pi/2} \frac{d\beta}{\sqrt{1 - \sin^2 \phi_0 \sin^2 \beta}} = K(\sin \phi_0)
 \end{aligned} \tag{3.11}$$

$$\begin{aligned}
 b &= \int_{\phi_0}^{\pi/2} \frac{d\alpha}{\sqrt{\sin^2 \alpha - \sin^2 \phi_0}} \\
 &= \int_0^{\pi/2} \frac{d\beta}{\sqrt{1 - \cos^2 \phi_0 \sin^2 \beta}} = K(\cos \phi_0)
 \end{aligned} \tag{3.12}$$

where $K(x)$ is a complete elliptic integral.

Since the lines of force BA and CD are perpendicular to the equipotential lines BC and AD, the electric field in the rectangle is uniform. It follows that

$$\Pi(\theta, \phi) = -\frac{jV_0}{2k} \left(1 + \frac{y_4}{b}\right) \tag{3.13}$$

After the substitution, in turn, of the several transformation, Π is finally obtained as a function of θ and ϕ . Once $\Pi(\theta, \phi)$ has been determined and by performing some mathematical manipulation the field equations become as [19]

$$\begin{aligned} E_{\theta}(r, \theta, \phi) &= -\frac{V_0 \cos\left[\frac{1}{2} \tan^{-1}(Y/X)\right] e^{-jkr}}{2b \sin \theta (X^2 + Y^2)^{1/4} r} \\ &= E_{\theta}(\theta, \phi) \frac{e^{-jkr}}{r} \end{aligned} \quad (3.14)$$

$$\begin{aligned} E_{\phi}(r, \theta, \phi) &= -\frac{V_0 \sin\left[\frac{1}{2} \tan^{-1}(Y/X)\right] e^{-jkr}}{2b \sin \theta (X^2 + Y^2)^{1/4} r} \\ &= E_{\phi}(\theta, \phi) \frac{e^{-jkr}}{r} \end{aligned} \quad (3.15)$$

$$\begin{aligned} H_{\theta}(r, \theta, \phi) &= -\frac{V_0 \sin\left[\frac{1}{2} \tan^{-1}(Y/X)\right] e^{-jkr}}{2bZ_c \sin \theta (X^2 + Y^2)^{1/4} r} \\ &= H_{\theta}(\theta, \phi) \frac{e^{-jkr}}{r} \\ &= -\frac{E_{\phi}(r, \theta, \phi)}{Z_c} \end{aligned} \quad (3.16)$$

$$\begin{aligned} H_{\phi}(r, \theta, \phi) &= -\frac{V_0 \cos\left[\frac{1}{2} \tan^{-1}(Y/X)\right] e^{-jkr}}{2bZ_c \sin \theta (X^2 + Y^2)^{1/4} r} \\ &= H_{\phi}(\theta, \phi) \frac{e^{-jkr}}{r} \\ &= \frac{E_{\theta}(r, \theta, \phi)}{Z_c} \end{aligned} \quad (3.17)$$

where $Z_c = 120\pi\Omega$ and $\tan^{-1}(Y/X)$ is multivalued when $Y \rightarrow 0$:

$$\tan^{-1}(Y/X) = \begin{cases} 0, & X > 0 \\ \pi, & X < 0 \end{cases} \quad (3.18)$$

X and Y are functions generated by conformal mapping and are given by

$$X = \sin^2 \phi_0 - 1/2 - 1/2(\cos 2\phi \cosh 2x_2) \quad (3.19)$$

$$Y = -1/2(\sin 2\phi \sinh 2x_2) \quad (3.20)$$

$$\text{where, } x_2 = \ln[\tan(\theta/2)\tan(\theta_0/2)] \quad (3.21)$$

From Eqn.(3.20) there are three roots for $Y = 0$. These are

Case- 1:

For $\phi = 0$: From Eqn. (3.19), it follows that $X = \sin^2 \phi_0 + 1/2(\cos 2x_2 - 1) > 0$, so that $\tan^{-1}(Y/X) = 0$ and Eqn.(3.14) and Eqn.(3.15) become as

$$E_\theta(\theta, \phi) = -\frac{V_0}{2b \sin \theta} \frac{1}{\sqrt{\sin^2 \phi_0 + \frac{1}{4} \left[\frac{\tan(\theta/2)}{\tan(\theta_0/2)} - \frac{\tan(\theta_0/2)}{\tan(\theta/2)} \right]^2}} \quad (3.22)$$

$$E_\phi(\theta, \phi) = 0 \quad (3.23)$$

Case- 2:

For $\phi = \pi/2$: From Eqn.(3.19), it follows that $X = \sin^2 \phi_0 - 1/2(\cos 2x_2 + 1) < 0$, so that $\tan^{-1}(Y/X) = \pi$ and

$$E_\theta(\theta, \pi/2) = 0 \quad (3.24)$$

$$E_\phi(\theta, \pi/2) = -\frac{V_0}{2b \sin \theta} \frac{1}{\sqrt{\frac{1}{4} \left[\frac{\tan(\theta/2)}{\tan(\theta_0/2)} + \frac{\tan(\theta_0/2)}{\tan(\theta/2)} \right]^2 - \sin^2 \phi_0}} \quad (3.25)$$

Case- 3:

For $\theta = \theta_0$ the value of X now depends on ϕ as $X = \sin^2 \phi_0 - \sin^2 \phi$

$$E_\theta(\theta_0, \phi) = \begin{cases} -\frac{V_0}{2b \sin \theta_0} \frac{1}{\sqrt{\sin^2 \phi_0 - \sin^2 \phi}}, \\ 0, \end{cases} \begin{cases} |\phi| < \phi_0 \text{ or } |\pi - \phi| < \phi_0 \\ |\phi| > \phi_0 \text{ or } |\pi - \phi| > \phi_0 \end{cases} \quad (3.26)$$

$$E_{\phi}(\theta_0, \phi) = \frac{0, \quad |\phi| < \phi_0 \quad \text{or} \quad |\pi - \phi| < \phi_0}{2b \sin \theta_0 \sqrt{\sin^2 \phi - \sin^2 \phi_0}}, \quad (3.27)$$

$$|\phi| > \phi_0 \quad \text{or} \quad |\pi - \phi| > \phi_0$$

3.2.2 Antenna Parameters

The antenna parameters such as field patterns, directivity, gain can be determined as follow:

3.2.2.1 Field Patterns

Generally there are three types of field pattern obtained from any antenna. These are:

Two patterns of orthogonal field components as a function of angle [$E_{\theta}(\theta, \phi)$ and $E_{\phi}(\theta, \phi)$] and pattern of the phase difference of these fields as a function of angle [$\delta(\theta, \phi)$]. A normalized field pattern can be obtained by dividing the field component by its maximum value. The normalized far field pattern of the electric field, E_{ϕ} is given as

$$E_{\phi}(\theta, \phi)_n = \frac{E_{\phi}(\theta, \phi)}{E_{\phi}(\theta, \phi)_{\max}}$$

The field patterns show that the electromagnetic field in the region $\theta < \theta_0$ is uniform and larger than that outside the cone ($\theta > \theta_0$). This property is very important for use with a directional EMP simulator. The field equations are free of frequency related term. Hence it can be treated as frequency independent antenna.

The field patterns of $E_{\theta}(\theta, \phi)$ at $\phi = 0$ are shown in the Fig.3.3 to Fig 3.6 for different θ_0 and ϕ_0 . It is shown from that figures the maximum radiation occurred at $\theta = 30^\circ$ and some weak field is present in the shadow region. The field patterns of $E_{\phi}(\theta, \pi/2)$ in plane $\phi = \pi/2$ shown in Fig.(3.7). It is shown that the maximum field exist at $\theta = 30^\circ$ and there is no weak field.

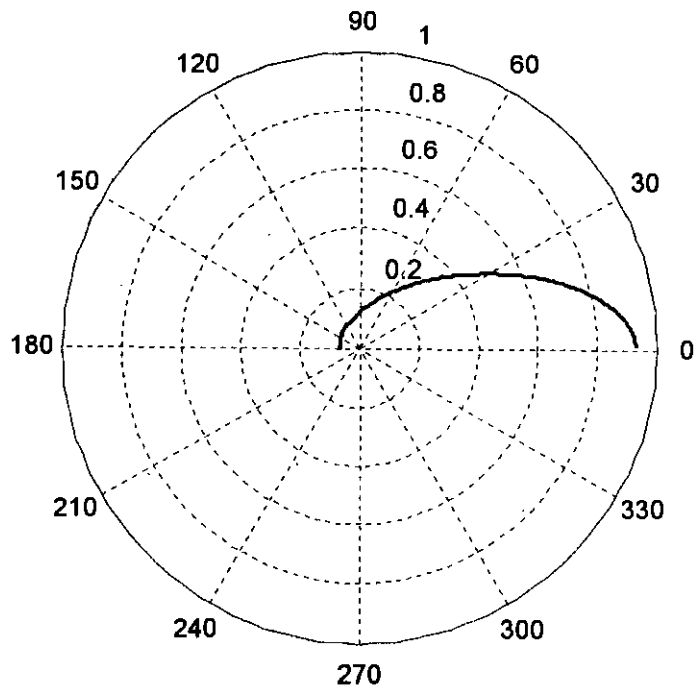


Fig3.3 Field pattern of $E_{\theta}(\theta, \phi)$ at $\theta_0=30^\circ$ and $\phi_0=89^\circ$ at the plane $\phi=0$.

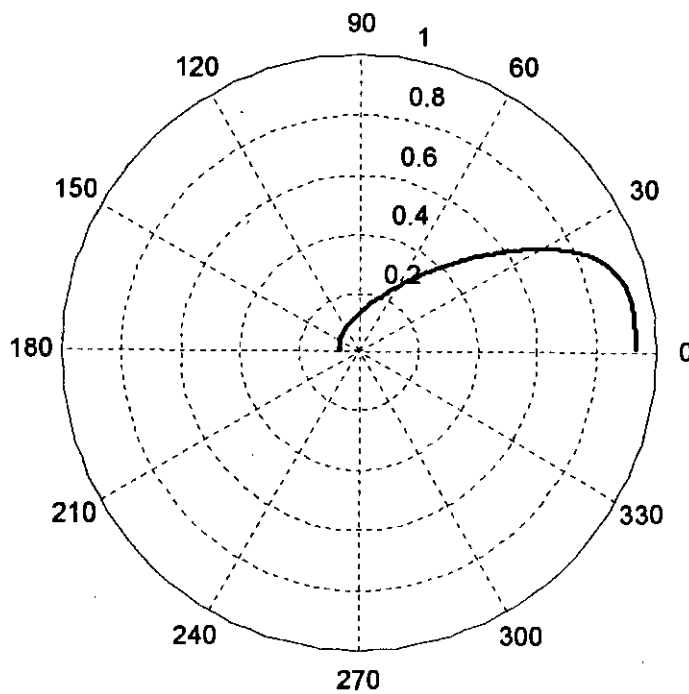


Fig3.4 Field pattern of $E_{\theta}(\theta, \phi)$ at $\theta_0=30^\circ$ and $\phi_0=45^\circ$ at the plane $\phi=0$.

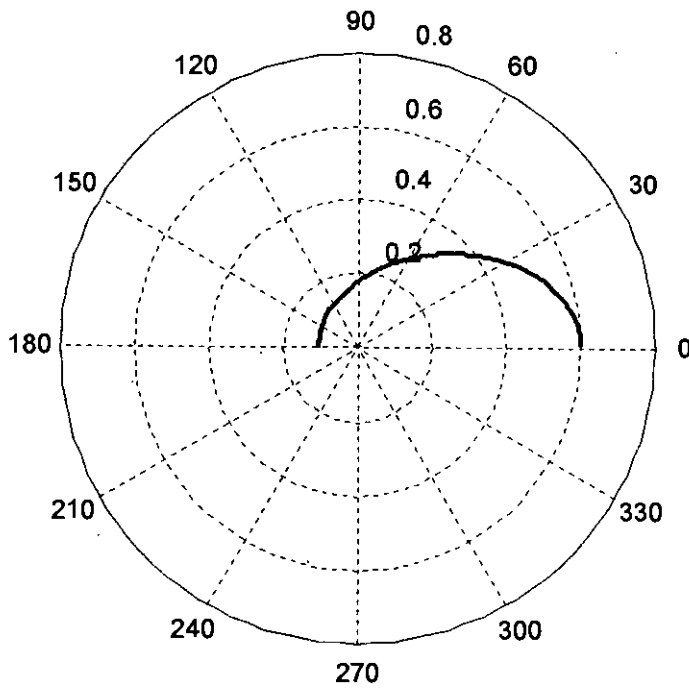


Fig3.5 Field pattern of $E_\theta(\theta, \phi)$ at $\theta_0 = 45^\circ$ and $\phi_0 = 89^\circ$ at the plane $\phi = 0$ plane.

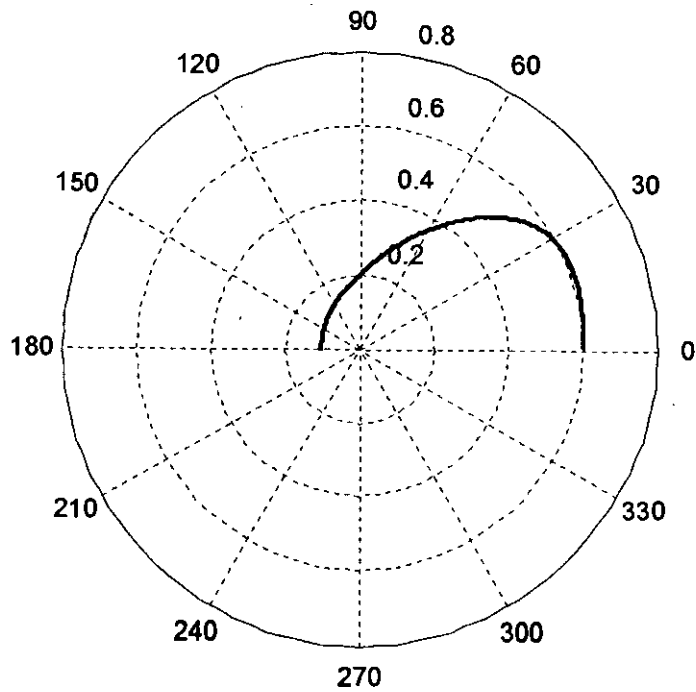


Fig3.6 Field pattern of $E_\theta(\theta, \phi)$ at $\theta_0 = 45^\circ$ and $\phi_0 = 45^\circ$ at the plane $\phi = 0$ plane.

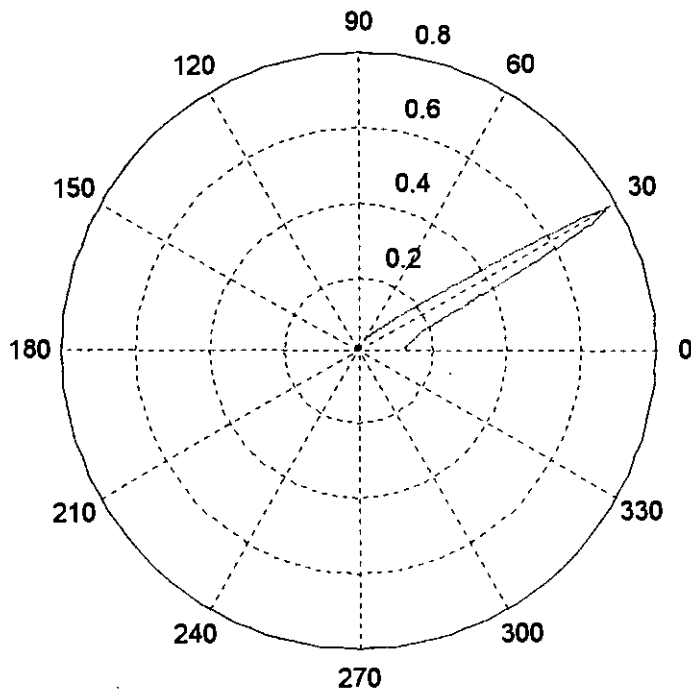


Fig3.7 Field pattern of $E_\phi(\theta, \pi/2)$ at $\theta_0=45^\circ$ and $\phi_0=89^\circ$ at the plane $\phi=\pi/2$ plane.

3.2.2.2 Directivity

Directivity is one of the most important figures-of-merit that describes the performance of an antenna. It is defined “as the ratio of the radiation intensity in a given direction from the antenna to the radiation intensity averaged over all direction”. It can be written as

$$D = \frac{U(\theta, \phi)}{U_0} = \frac{4\pi U(\theta, \phi)}{P_r} \quad (3.28)$$

Where, $U(\theta, \phi)$ is the radiation intensity in the direction of (θ, ϕ) and P_r is the radiated power.

If the direction is not specified, it implies the direction of maximum radiation intensity (maximum directivity) expressed as

$$D_0 = \frac{U_m(\theta, \phi)}{U_0} = \frac{4\pi U_m(\theta, \phi)}{P_r} \quad (3.29)$$

The determination of directivity begins with the calculation of the total power radiated by the antenna, which requires knowledge of the average Poynting Vector, S_r at a distant point from the antenna. We know

$$S_r = \frac{1}{2} \Re(\bar{E} \times \bar{H}^*) \quad (3.30)$$

$$\bar{E} = E_r \cdot \hat{a}_r + E_\theta \cdot \hat{a}_\theta + E_\phi \cdot \hat{a}_\phi \quad (3.31)$$

$$\bar{H} = H_r \cdot \hat{a}_r + H_\theta \cdot \hat{a}_\theta + H_\phi \cdot \hat{a}_\phi \quad (3.32)$$

But r and θ components of H are equal to zero. Hence

$$\bar{E} = E_{\theta} \cdot \hat{a}_{\theta} \quad (3.33)$$

$$\bar{H} = H_{\phi} \cdot \hat{a}_{\phi} \quad (3.34)$$

$$\begin{aligned} \text{Therefore, } \bar{E} \times \bar{H} &= E_{\theta} H_{\phi} (\hat{a}_{\theta} \times \hat{a}_{\phi}) \\ &= E_{\theta} H_{\phi} \hat{a}_r \end{aligned} \quad (3.35)$$

$$E_{\theta} = \frac{V_0}{2b \sin \theta} \frac{1}{\sqrt{\frac{1}{4} \left[\frac{\tan(\theta/2)}{\tan(\theta_0/2)} - \frac{\tan(\theta_0/2)}{\tan(\theta/2)} \right]^2 + \sin^2 \phi_0}} \quad (3.36)$$

$$H_{\phi} = \frac{V_0}{2b \sin \theta} \frac{1}{\sqrt{\frac{1}{4} \left[\frac{\tan(\theta/2)}{\tan(\theta_0/2)} - \frac{\tan(\theta_0/2)}{\tan(\theta/2)} \right]^2 + \sin^2 \phi_0}} \quad (3.37)$$

Substituting the Eqn.(3.36) and Eqn.(3.37) into the Eqn.(3.30) and solving for S_r and P_r one can get

$$S_r = \frac{1}{2} \frac{V_0^2}{4b^2 Z_c \sin^2 \theta \left\{ \frac{1}{4} \left[\frac{\tan(\theta/2)}{\tan(\theta_0/2)} - \frac{\tan(\theta_0/2)}{\tan(\theta/2)} \right]^2 + \sin^2 \phi_0 \right\}} \quad (3.38)$$

and

$$P_r = \int_{\theta=0}^{\pi} \int_{\phi=0}^{\pi/2} S_r r^2 \sin \theta d\theta d\phi \quad (3.39)$$

If the direction of radiation intensity is not specified, then the radiation intensity implies the direction of maximum intensity [3].

The maximum intensity occurred when $\theta_0 = \theta$. Hence

$$E_{\theta}(\text{max}) = \frac{V_0}{2b \sin \theta \sin \phi_0} \quad (3.40)$$

$$H_{\phi}(\text{max}) = \frac{V_0}{2b Z_c \sin \theta \sin \phi_0} \quad (3.41)$$

$$\therefore S_r = \frac{V_0^2}{8b^2 Z_c \sin^2 \theta \sin^2 \phi_0} \quad (3.42)$$

$$U_m(\theta, \phi) = \int_{\theta=0}^{\pi} \int_{\phi=0}^{\pi/2} S_r r^2 \sin \theta d\theta d\phi \quad (3.43)$$

It is the average power, $U(\theta, \phi)$ and it can be find by solving above equation by any numerical integration technique within certain limit. In this work well-known Simpson's rule is used for integration. By solving Eqn.(3.29), Eqn(3.39). and Eqn(3.43), one can get the directivity of the antenna. In this work MATLAB is used, to get the directivity and it is maximum at $\theta = 30^\circ$ and it is 16.5.

3.2.2.3 Gain

The gain of an antenna can be expressed in terms of the directivity (where directivity is measured in the direction of maximum intensity) and the radiation efficiency as given below

$$G = \eta_r D \quad (3.44)$$

Where η_r is the radiation efficiency which can be obtained as

$$\eta_r = \frac{R_r}{R_r + R_{ohmic} + R_{ref}} \quad (3.45)$$

Where R_r = radiation resistance
 R_{ohmic} = ohmic resistance
 R_{ref} = reflector resistance

3.3 DESIGN PARAMETERS OF VCA

As said earlier, the two angles, namely the semi-vertical angle and the azimuth structural angle are mainly the parameters that are to be selected through calculation for desired field structure and strength. These two angles are described in the following paragraphs.

3.3.1 Semi-vertical Angle

It is desirable that the diameter of the base of the cone as wide as to cover the whole width of the sheet so that it can give a complete assessment of the shielding capability of the test material.

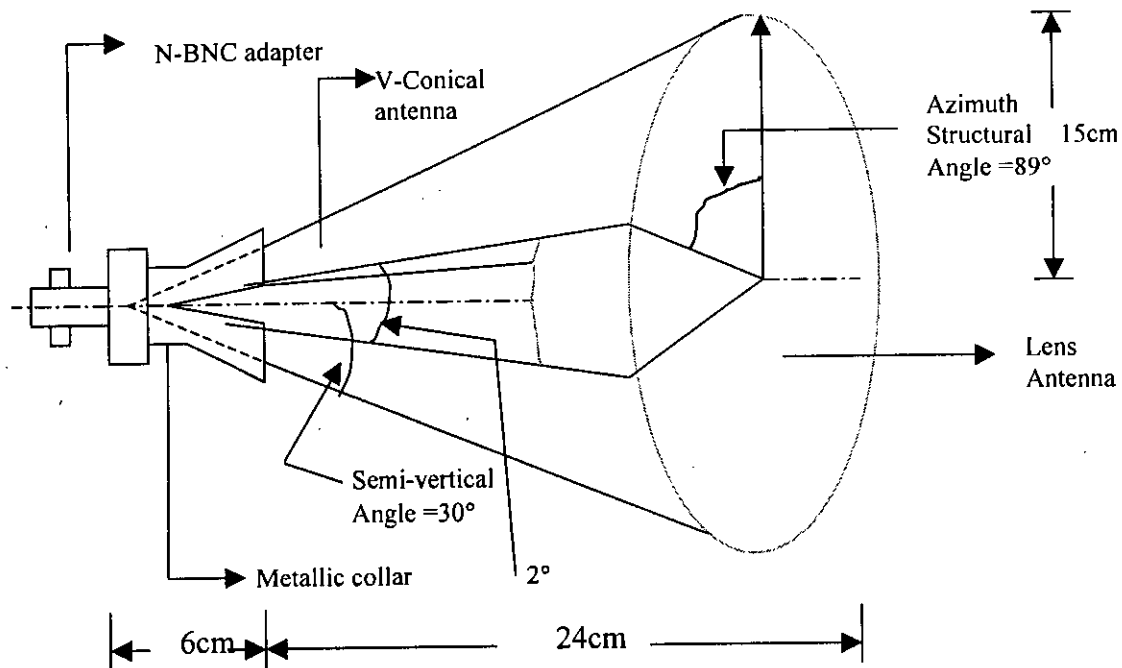


Fig. 3.8 V-conical Lens Antenna Assembly

The length and volume of the cone would be excessively large even if its base were equal to the minimum sheet width. As a compromise the base could be chosen to be half the width of the sheet. In that case the measurements would relate to approximately 50% of the sheet, which is probably adequate for a typical on-line monitoring system. The Fig.3.8 V-Conical Lens antenna assembly for on-line SE measurement.

When base diameter is selected, it is desirable to keep the VCA as short as possible. Because, the narrower the semi-vertical angle the longer the VCA would be, which will be very difficult from the mechanical point of view and complex to manufacture the VCA. Thus a compromise is to be made. In present SE measurement the ratio of h/D where h is the height of the cone and D is the diameter of the base is selected to be very close to unity. In present case, the base diameter is 30cm and the semi-vertical angle is 30° , then the height is 26 cm, thus satisfying the above aspect ratio requirement.

3.3.2 Azimuth Structural Angle

The characteristic impedance of the antenna is dependent on the azimuth structural angle, denoted by Φ_0 . The input impedance of the antenna is given by [19]

$$Z_{in} = \frac{\eta_0}{2} \frac{K(\cos \phi_0)}{K(\sin \phi_0)} \quad (3.46)$$

Where, $K(k)$ is the complete elliptic integral of first kind of modulus k
 η_0 is the free space intrinsic impedance.

It is desirable to make Z_{in} as close as possible to 50Ω . It has been found that for $\phi_0 > 89^\circ$, Z_{in} becomes approximately 50Ω . Of course, ϕ_0 must be less than 90° . With such a large value of ϕ_0 , there is another advantage in that the leakage of the test field and possibility of infringement of the indirect path signal into the test device will be very small.

3.4 CONSTRUCTION OF VCA

The construction of VCA with very stringent angular specifications is quite difficult. It may be fabricated from plain sheet metals or it may be machined from a block of material. In present SE measurement, VCA is fabricated from a aluminium sheet of thickness 0.7mm. This technique reduces the cost of both material and labour. Selection of the thickness of the sheet is not crucial. Adequate shielding capability and the ease of mechanical handling are the factors to be considered. The construction work for VCA may be divided in steps which are given in the following subsections.

3.4.1 Fabrication of the Cone

The cone is formed from a semi-circular sheet of aluminium and then cut a longitudinal tapered slot at the middle, meeting the requirement of azimuth structural angle $\Phi_0 = 89^\circ$. The slant height of the cone will be the radius of the semi-circle. The slant height of the cone can be determined from the semi-vertical angle, height of the cone and the radius of

the base. Slant height of the cone is 26cm. A metallic conical frame is essential to hold the shape of the cone which can be machined from a cylindrical block of aluminium. An insulator is set into the inside portion of the frame in order to electrically separate the VCA from the frame. The frame and VCA is assembled by nylon screws of M₃ size. The tapered end of this frame should be terminated with a threaded cylindrical collar which further terminated with a circular threaded metallic knob where the N-BNC adopter can be fitted. The height of the cylindrical collar plus thickness of the circular knob should be such that if the standard N-connector would be exactly at the vertex of the cone.

3.4.2 Feed Arrangement

The centre stud of the coaxial N-connector can be employed as a mono-pole antenna protruding into the cone to feed it and this is the usual procedure of feeding wave guides. The generation of the spherical TEM wave even in the near region of the cone can only be insured, if the requirement of the existence of a point source at the vertex of the cone can be satisfied. This can be achieved if the pointed tip of the centre stud of the N-BNC adopter can be placed at the vertex of the cone. A feed arrangement is shown in Fig.3.9.

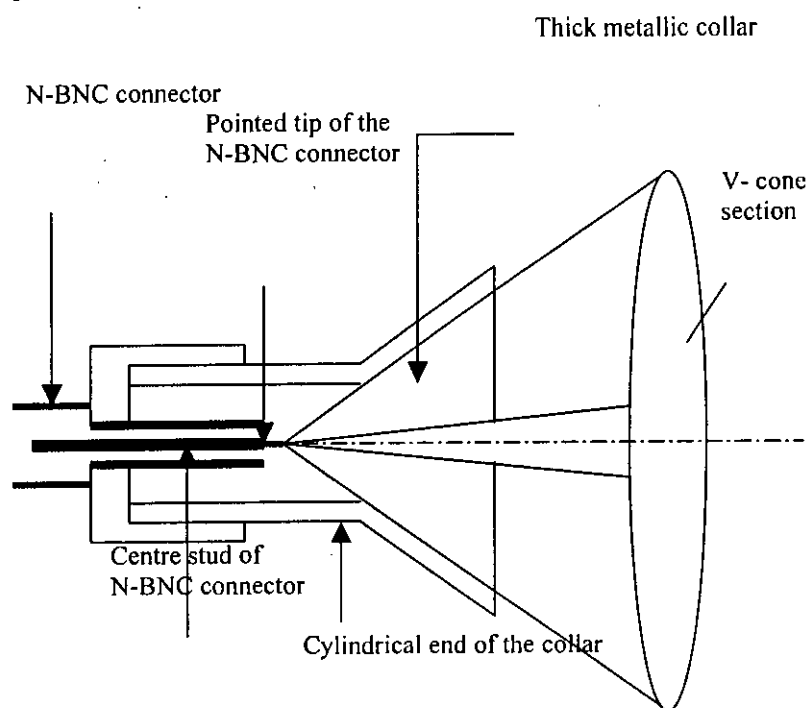


Fig.3.9 Feed arrangement of VCA

3.5 LENS ANTENNA

The inaccuracies in RF and microwave measurements using free space methods are mainly due to the diffraction effects at the edges of the sample and distortion of the test field caused by the probable scattering from nearby objects. The possibility of background interference is also an important factor to be compared in such measurements. Horn-lens combinations can be used for electrical characterization (dielectric constant measurement) of composite materials in free-space measurements at microwave frequencies from 5.85 – 40 GHz. In those applications, the above mentioned limitations of free space measurements can be successfully overcome by using lens antenna in front of a VCA [22].

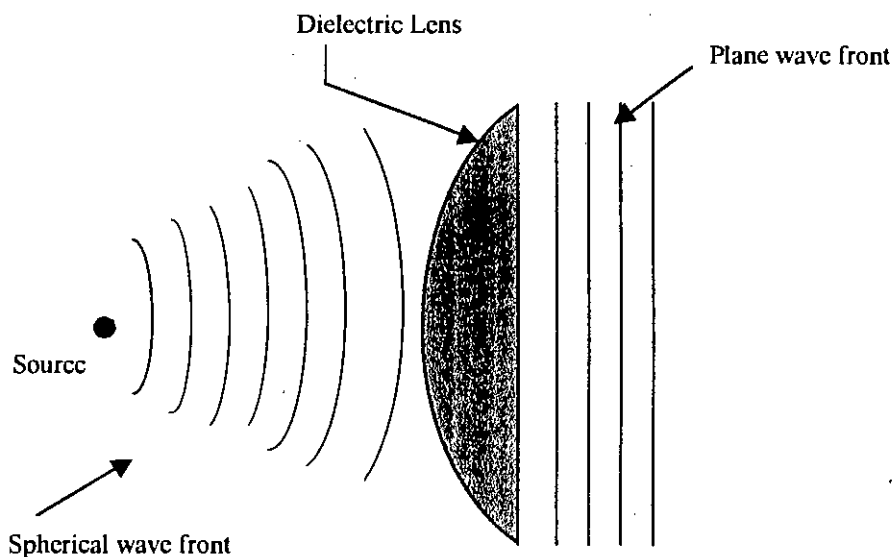


Fig.3.10 Transformation of spherical wave front into plane wave front while passing through the lens antenna [22].

Lens antennas may be divided into two distinct types, (1) delay lenses, in which the electrical path length is increased by the lens medium, and (2) fast lenses, in which the

electrical path length is decreased by the lens medium. In delay lenses the wave is retarded by the lens medium. Dielectric lenses and H-plane metal-plate lenses are of the delay type. Plano-convex lens is also a delay type lens. Because when the wave front incident on convex surface then, it will be delayed. The dielectric lenses are divided into two groups:

1. lenses constructed of nonmetallic dielectrics, such as lucite or polystyrene.
2. Lenses constructed of metallic or artificial dielectrics.

In present research a VCA of aluminium is applied for simulating the spherical wave front of a TEM wave which is then transformed into a plane wave front as in Fig 3.10 by the use of a dielectric lens antenna of nylon fitted at the face of the VCA. The dielectric lens is used here because of its light weight and good performance with the reflector type antenna such as VCA. The use of a lens antenna would substantially reduce the size of the test system compared to that required if conventional test methods were used for the same frequency band . However, it would provide plane wave in a confined area so that the possibility of indirect path signal reaching the receiving antenna can be reduced significantly.

3.6 LIMITATIONS OF THE LENS ANTENNA

In lens antennas the primary antenna does not interfere with the plane wave leaving the aperture as it does in a symmetrical parabolic reflector antenna [3]. However, the energy reflected from the lens surfaces may be sufficient to cause a mismatch of the primary antenna to its feed line or guide. In the lens Fig. 3.11 reflections from the convex surface of the lens do not return to the source except from points at or near the axis. This is not serious, but the wave reflected internally from the plane lens surface is refocused at the primary antenna and be disturbing. In this case, the wave is reflected at normal incidence, and the reflection coefficient is

$$\rho = \frac{n-1}{n+1} \quad (3.47)$$

where, n = refractive index of the dielectric lens material which is the ratio of the intrinsic impedance of free space (Z_0) and the intrinsic impedance of the dielectric lens (Z). The intrinsic impedance of the dielectric lens depends on its relative permittivity and relative permeability.

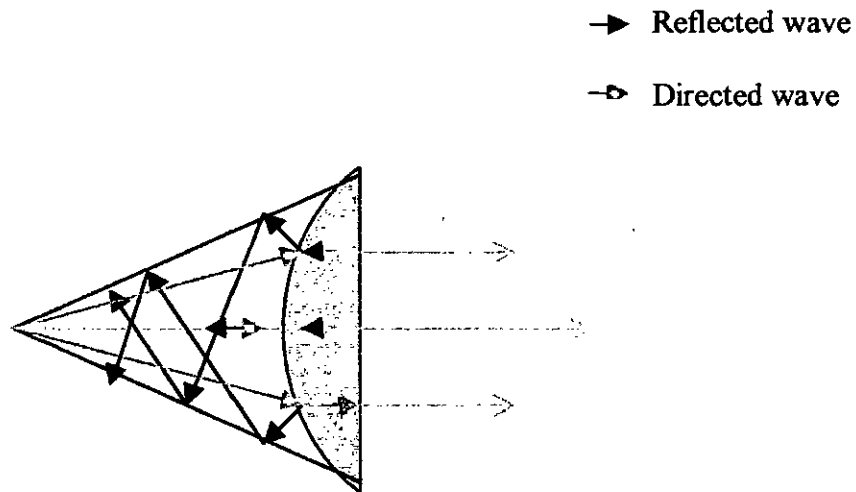


Fig 3.11 Effect of reflections in the air-lens interfaces [22].

In order to reduce the reflection the air-lens impedance mismatch is to be minimized. Hence, for small reflection low refractive index is desirable, which is possible, if dielectric materials of small ϵ_r is used (such as nylon) or if magneto-dielectric materials whose permittivity and permeability are very close to each other, are used for constructing the lens. In present work, nylon lens is used which refractive index 1.55 because of its availability in market..

Non-uniformity of the field emerging from the flat face of the lens is due to the difference in physical path length traveled by EM rays at different height of the lens. It can be avoided by letting the waves suffer a definite amount of penetration loss, while passing through the lens. Selection of a magneto-dielectric material could thus contribute to the elimination of this problem as well.

3.7 DESIGN PARAMETERS FOR LENS ANTENNA

The plano-convex lens is designed on the basis of Fermat's Principle which is ray analysis methods of geometrical optics. The principle is that the equality of electrical path length of different rays whatever may be the constituent material of the lens. In present SE measurement it is desirable to determine the shape of the plano-convex lens of Fig.3.12 for transforming the spherical wave front from an isotropic point source or primary antenna into a plane wave front. The origin of the co-ordinate axes is chosen at the vertex of the cone and the X-axis is the axis of the cone. The field over the plane surface can be made everywhere in phase by shaping the lens so that all paths from the source to the plane are of equal electrical length. Thus in Fig.3.12 the electrical length of the path OPP' must be equal to the electrical length of the path $OQQ'Q''$, or more simply OP must equal OQ' . Let $OQ=L$ and $OP=R$ and let the medium surrounding the lens be air or vacuum. Then

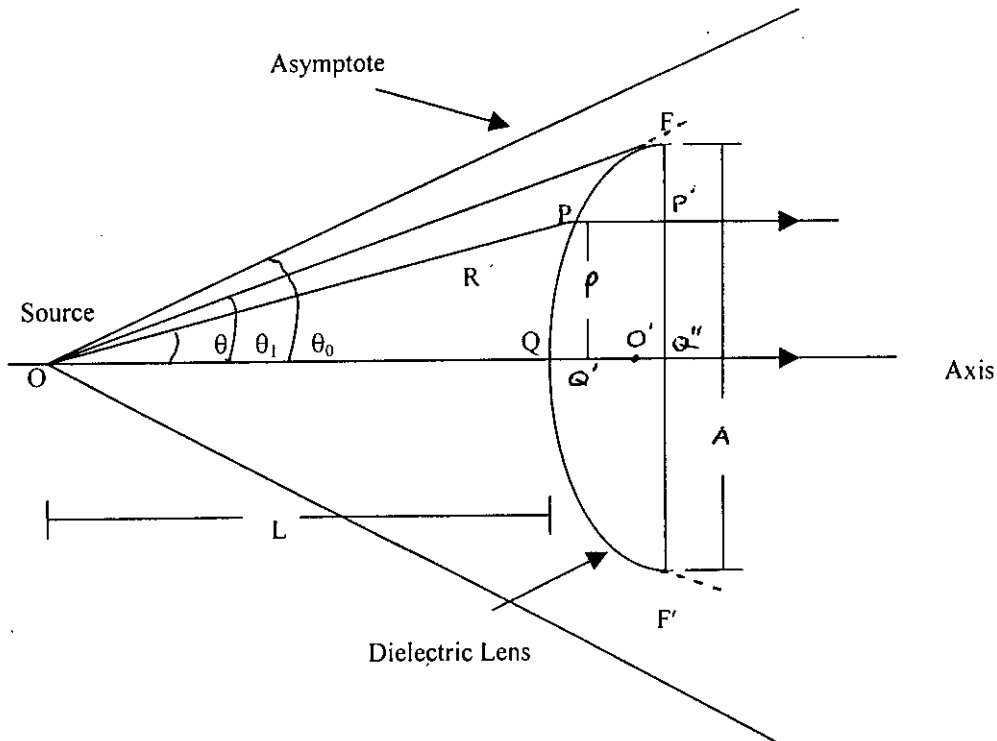


Fig.3.12 Path lengths in dielectric Lens.

$$\frac{R}{\lambda_o} = \frac{L}{\lambda_o} + \frac{R \cos \theta - L}{\lambda_d} \quad (3.48)$$

Where, $R \rightarrow \sqrt{(x^2 + y^2)}$
 $y^2 \rightarrow (n^2 - 1)x^2 - 2xnL(n-1) + (n-1)^2 L^2$
 $n \rightarrow$ refractive index of the lens material $= \lambda_o / \lambda_d$

Now multiplying (1) by λ_o and solving for R

$$R = \frac{(n-1)L}{n \cos \theta - 1} \quad (3.49)$$

Fig. 3.13 Geometry of the lens antenna fixed at the face of the VCLA [22].

This represents an equation of a hyperbola which gives the required shape of the lens. Reference to Fig. 3.12 the distance L is the focal length of the lens. The asymptotes of the hyperbola are at an angle θ_0 with respect to the axis.

One of the major design criteria is that the focus length L plus the depth of the lens should be to the height of the cone. Moreover, to fit lens at the mouth of the V-cone

antenna, it is essential that the diameter of the flat face of the lens is equal to the diameter of the base of the cone.

In fine it may be said that the designing parameters of the lens antenna are

- (1) The curved face of the lens should be a hyperbola.
- (2) The focal length of the lens plus its depth should be equal to the height of the cone.
- (3) The diameter of the flat face of the lens should be equal to the diameter of the base of the cone.

3.8 CONSTRUCTION OF DIELECTRIC LENS

The lens to be used in front of the VCA would be a section of a spherical hyperbola and the origin, it can be assumed to be a point source at the focus of that hyperbolic surface. Selection of material and fitting onto the VCA are the main steps to be taken in the construction of the lens.

3.8.1 Selection of Material

In the construction of lens non-metallic dielectrics, artificial dielectrics or metallic parallel plates may be used. Dielectric materials, such as nylon or polystyrene are preferable. Because a bulk piece of such a material can be readily machined to give the particular hyperbolic shape. But reflections from the lens interface and non-uniformity of field emerging from the lens are the major limitations of this dielectric lens. In our present SE measurement nylon (polyamide) is used. Non-uniformity may be reduced by using lossy dielectric instead of nylon. Reflectivity and non-uniformity problems may be reduced by using magneto-dielectric materials.

In the case of artificial dielectric, the constituent material itself has to be designed and manufactured following some stringent conditions.

In case of metallic parallel plates lens, the attachment to the open face of the VCA is very difficult as a constant separation between the plates is to be maintained. Moreover, every single constituent plate requires specific and individual dimensions which is very difficult to maintain.

3.8.2 Fitting on to the VCA

There should be a frustum section near the flat face of the lens antenna so that the VCA can be screwed onto that section as Fig3.14. The dimension of the frustum section should be

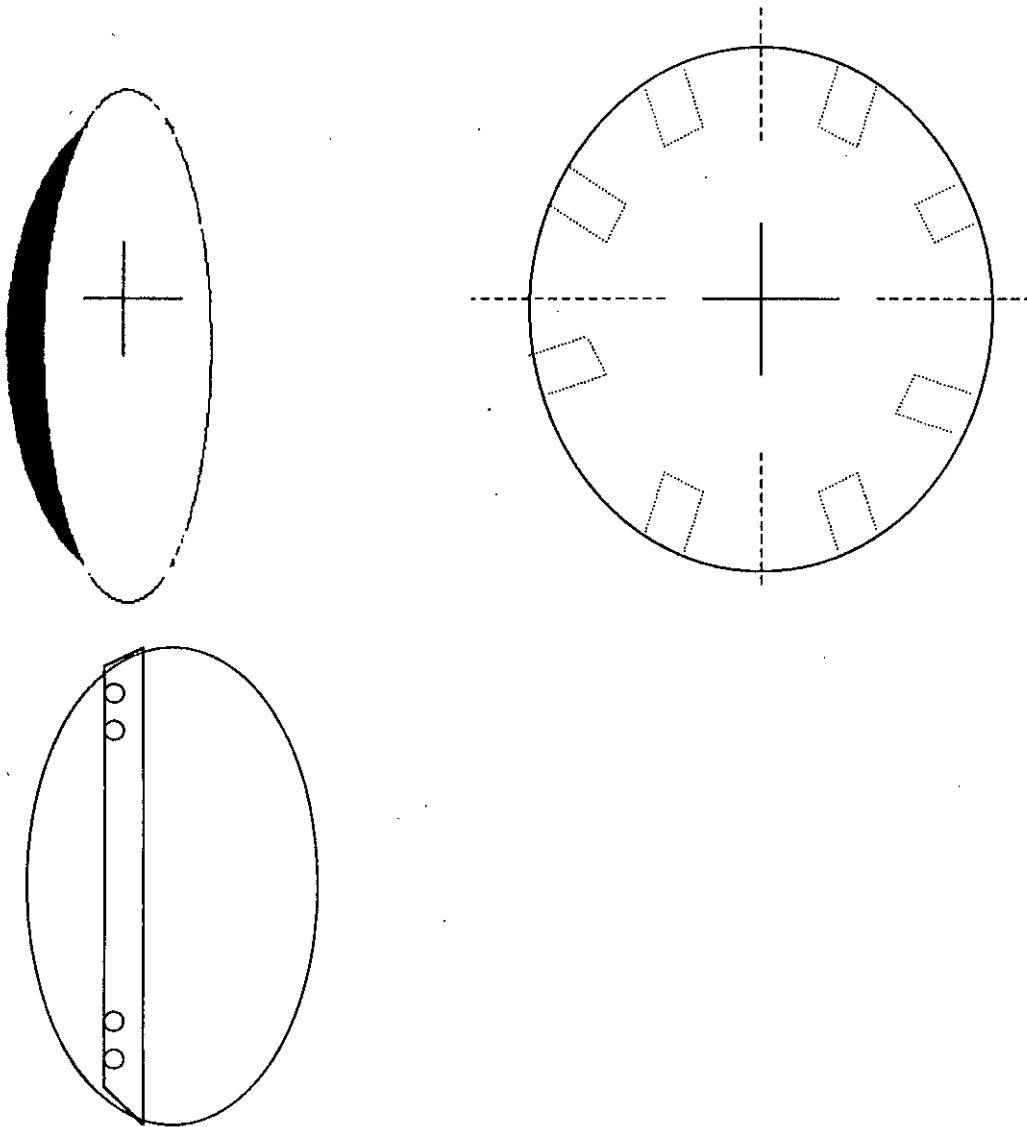


Fig.3.14 Constructional details of the dielectric lens (not in scale) [22].

such that it push-fits into the VCA. Around the frustum, threaded holes are to be provided radially for screwing the VCA with the lens by using 3mm screws.

3.9 V-CONICAL ANTENNA IN FRONT OF A LENS

The generation of standard test fields, which fulfil the requirements of emission and susceptibility measurements, largely depend on the strict maintenance of the design specifications of the test device. There are two parts in this type of antenna. These are (1) V-Conical Antenna (VCA) (2) a dielectric lens antenna in front of the VCA. In order to design a VCA only two angular dimensions are needed to be maintained carefully [19]. But its feed network must be well designed so that the requirement of a point source at the tip of the cone can be fulfilled precisely.

The lens antenna which is to be used in conjunction with VCA to simulate a far-field situation, requires careful design analysis to minimize reflections from the lens-air interface as well as to obtain the uniformity of the plane wave in front of it.

In present SE measurement, a pair of VCA to be used, where one acts as a transmitter and the other as a receiver. A compromise is to be made in design of a VCA. This is due to the fact that if the diameter of the base of the cone is very small compared to the width of the MUT, the test result would represent only a very small portion of the MUT. Meanwhile, if it is made very large, the size of the lens (antenna) would be colossal incurring manufacturing complexity. Moreover, to maintain a narrow apex with base diameter, the height of the cone would be awkwardly large.

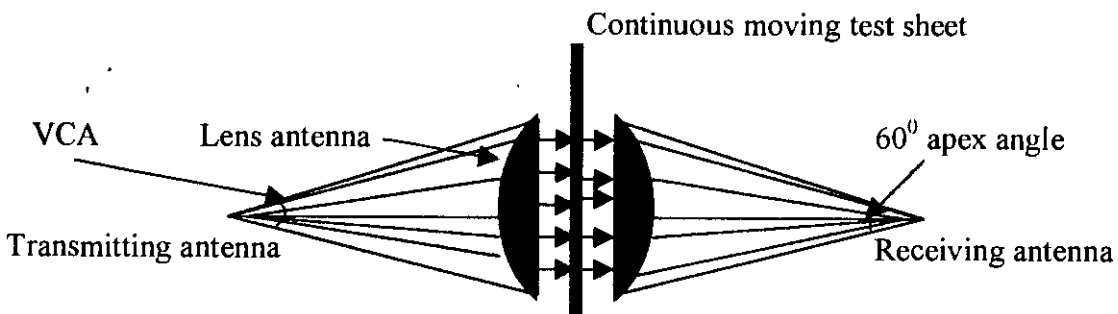


Fig.3.15 V-Conical lens antenna assembly for on-line SE measurement [22].



CHAPTER 4

ANTENNA MEASUREMENT AND SHIELDING EFFECTIVENESS MEASUREMENT

 **INTRODUCTION**

 **TEST SET UP FOR RADIATION PATTERN MEASUREMENT**

 **INSTRUMENT AND OTHER ACCESSORIES FOR FIELD
MEASUREMENT**

 **FEED ARRANGEMENT**

 **MEASUREMENT PROCEDURE**

 **TEST RESULT AND COMPARISON OF ANTENNA**

PARAMETERS WITH THE THEORETICAL RESULT

 **SE MEASUREMENT**

CHAPTER –4

ANTENNA MEASUREMENT AND SHIELDING EFFECTIVENESS MEASUREMENT

4.1 INTRODUCTION

Efficient radiation from the VCLA in the desired frequency range depends on the size and shape of the antenna. The developed EMC antenna is used to measure the SE of different types of materials. EMC measurement depends on types of MUT, measurement techniques, types of incident field i.e. sources of EMI, test site and measuring instruments. The SE values differ widely due to reflection, absorption, and successive re-reflections inside the MUT sheet.

In this chapter a brief description of test set up is given in section 4.2. Instrument and other accessories are presented in section 4.3. Feed arrangement for measurement of antenna parameters is given in section 4.4. Procedure of antenna parameter measurement is described briefly in section 4.5. A comparison between theoretical results and measured results of antenna parameters is stated in section 4.6. In section 4.7 SE measurement of test samples and their comparison are briefly described.

4.2 TEST SET UP FOR ANTENNA RADIATION PATTERN MEASUREMENT

It is assumed that the developed EMC antenna satisfies the reciprocity theorem and hence two VCLAs of the same dimensions are constructed to experimentally observe the radiation pattern of the antennas. One is used as a transmitting antenna and the other is used as a receiving antenna. Schematic block diagram of the test set up and a photograph of the test set up is shown in Fig. 4.1 and Fig. 4.2 respectively.

The receiving antenna is placed on a bench to rotate it by manually in the horizontal plane by varying the polar angle at $\theta_0=30^\circ$. The angular position of this

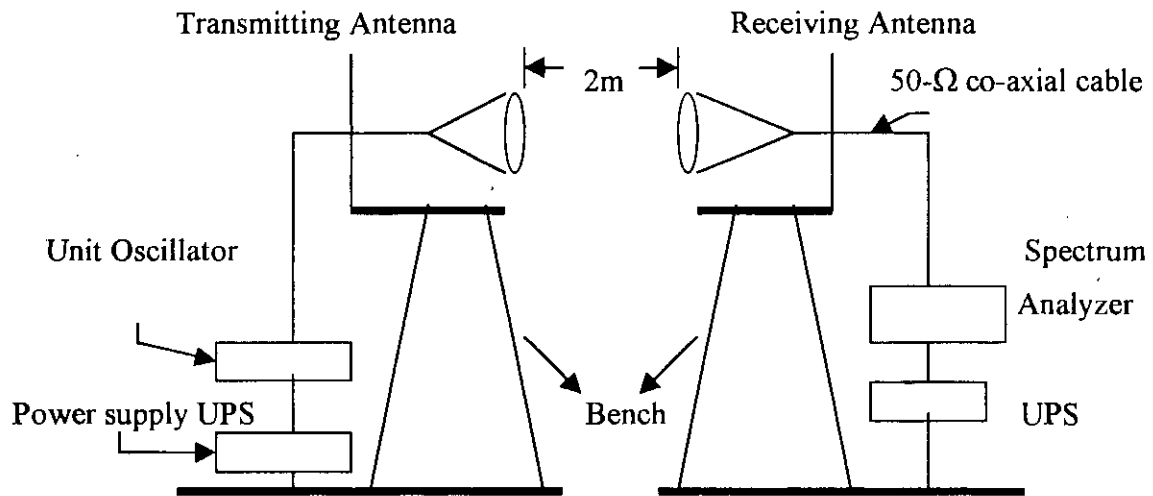


Fig 4.1 Field Measurement Set Up.

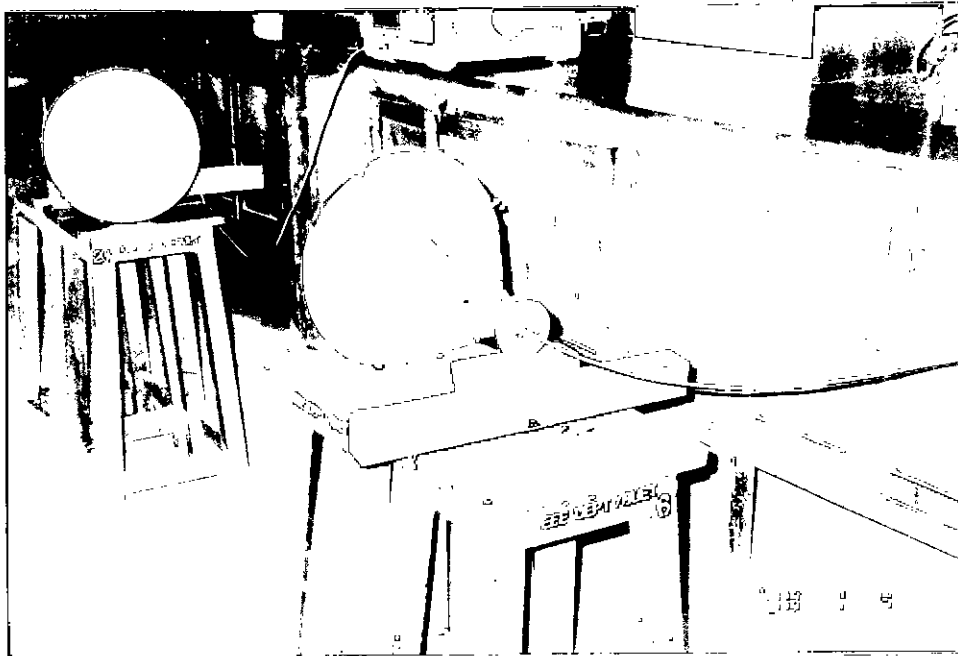


Fig.4.2 Photograph of the test set up.

antenna is determined by pasting a polar diagram on the bench on which one can rotate the antenna at 15° step according to the polar diagram. The input signal is fed into the end of the N- BNC connector of the transmitting antenna from a unit oscillator by a $50\text{-}\Omega$ co-axial cable. On the other hand the output signal of receiving antenna is fed into a spectrum analyzer for the measurement of field received by the antenna.

4.3 INSTRUMENT AND OTHER ACCESSORIES FOR FIELD MEASUREMENT

Basic instruments for the field measurement include unit oscillator with in-built IF amplifier and a spectrum analyzer. The unit oscillator is used to feed the RF signal into the transmitting antenna. At the receiving side the spectrum analyzer is used to measure the field strength. Accessories include $50\text{-}\Omega$ co-axial cable Power supply, UPS for Spectrum analyzer and $50\text{-}\Omega$ male and female N-BNC connectors. Some relevant features of the unit oscillator, and spectrum analyzer are given in following subsections.

4.3.1 Unit Oscillator:

One General Electric Company Unit Oscillator is used as a signal generator. The frequency range of this unit oscillator can be varied from 250 MHz to 900 MHz.

4.3.2 Spectrum Analyzer:

The spectrum analyzer of Agilent Technology is a portable instrument and requires no physical installation other than connection of a power source. There is no need to select a line voltage. The required line voltage is 195 – 250 Vrms (47 to 60 Hz) and power consumption is less than 300 W. It is a sophisticated instrument to measure the signal strength directly from its monitor. There is no need for pre-alignment.

4.4 FEED ARRANGEMENT

A photograph of the feeding arrangement with the load connections is shown in Fig 4.3. RF signal is to be fed into the transmitting antenna from unit oscillator by a 50- Ω co-axial cable which is terminated by a female 50- Ω N-BNC connector and then it is fed into the antenna by a male 50- Ω BNC connector.

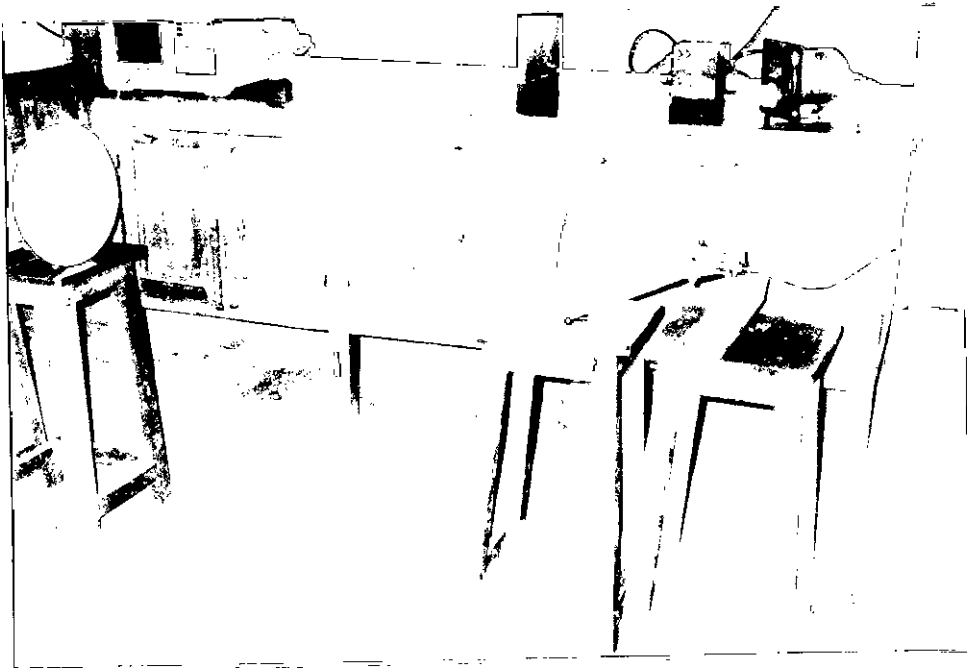


Fig 4.3 Photograph of Feed arrangement with the load connections.

4.5 MEASUREMENT PROCEDURE

Field measurement is done at a distance of 3 meter and 2 meter at different frequencies. In order to obtain horizontal pattern, the receiving antenna is rotated in the horizontal plane where the azimuth angle (ϕ) varies from 0 to 180°.

The receiving antenna rotated to obtain the maximum field strength, which is found at $\phi=89^\circ$ and $\theta_0=30^\circ$. The position of maximum field strength is then considered as the reference position for this work. The radiated EM field is recorded by rotating the receiving antenna in 15° steps.

4.6 TEST RESULT AND COMPARISON OF ANTENNA PARAMETERS

4.6.1 Radiation Pattern

Radiation pattern is the field pattern showing the variation of the electric field intensity at a constant radius as a function of polar co-ordinate. It has already been mentioned in the previous chapter that the VCLA radiates in the azimuth angle (ϕ) varying from 0° to 90° in the horizontal plane with poor field from 90° to 180° . In this work the reference position is considered at $\phi=89^\circ$ and $\theta_0=30^\circ$. Therefore, the presence of the radiated field is to be expected in between $\phi \geq 0^\circ$ and $\phi \leq 90^\circ$ in the same plane. The maximum field is to be expected at $\theta=30^\circ$. The measured field strengths at different position of the transmitting antenna are normalized by the maximum field strength. Polar plots of the measured radiated fields drawn by MATLAB are shown in Fig. 4.4 to Fig 4.8. The theoretical pattern and the measured pattern are almost identical but a weak field is found in the shadow region. The maximum field strength is found at $\theta_0=30^\circ$ which is consistent with theoretical result. However, in some cases field patterns are found to be distorted and maximum field is found in more than one position.(Fig 4.7 and Fig.4.8). These may be due to the reflections from the metallic objects present in the room and associated cabling, radiation from the instruments, reception of the other EM noise by both the receiving and transmitting antennas, the leakage current flowing through the reflector which also contributes to radiation. The distortion in the field may also be due to edge diffraction. Change in amplitude of the unit oscillator during measurement can cause distortion in the radiation pattern.

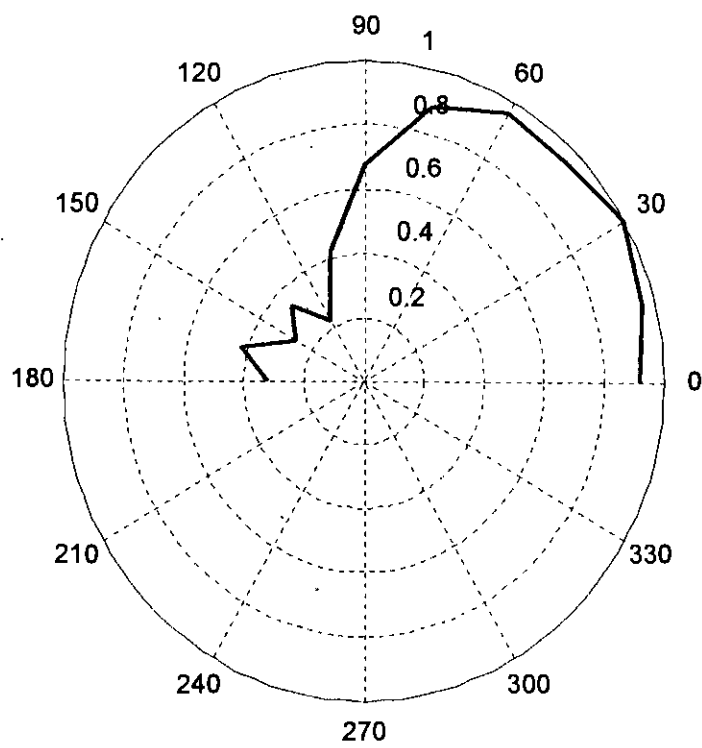


Fig 4.4 Normalized Radiation Pattern at 2m distance ($f = 300$ MHz).

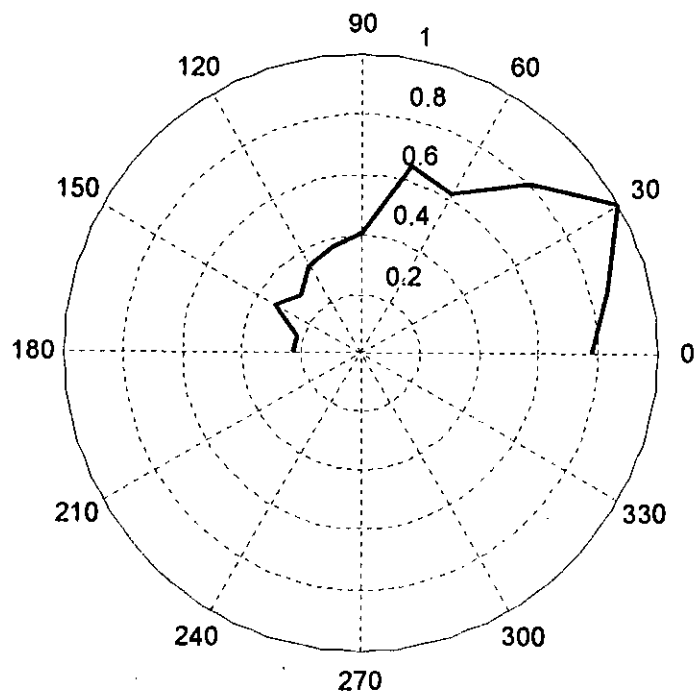


Fig.4.5 Normalized Radiation Pattern at 2m distance ($f = 450$ MHz).

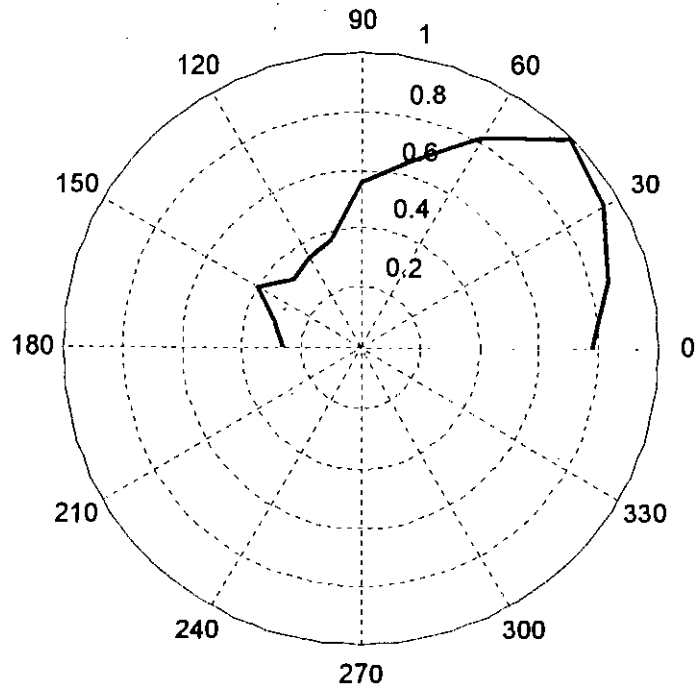


Fig.4.6 Normalized Radiation Pattern at 3m distance ($f = 300$ MHz).

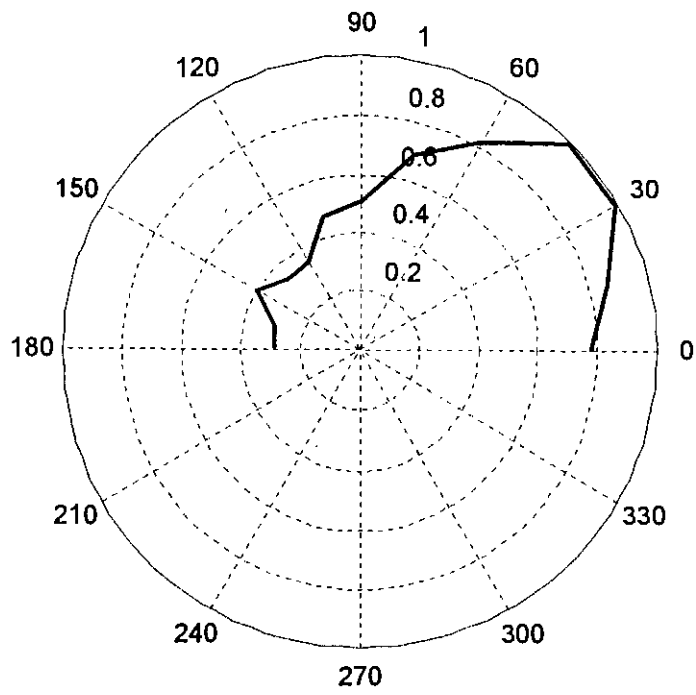


Fig.4.7 Normalized Radiation Pattern at 3m distance ($f = 450$ MHz).

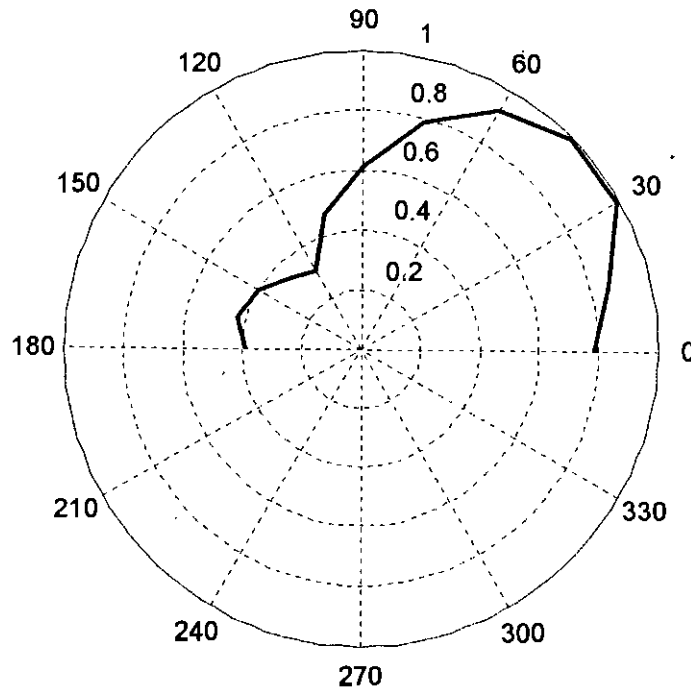


Fig.4.8 Normalized Radiation Pattern at 3m distance ($f = 600$ MHz).

4.6.2 Gain

The most important figure-of-merit that describes the performance of a radiator is the gain. There are various techniques and antenna ranges that are used to measure the gain. Usually there are two methods that can be used to measure the gain of an electromagnetic radiator: absolute-gain and gain-transfer (or gain-comparison) measurements. In absolute gain measurement two antenna method is very popular. Because it is universally accepted

[21]. All these methods are based on Friis transmission formula which assumes that the measuring system employs, each time, two antennas. The antennas are separated by a distance R , and it must satisfy the far-field criterion of each antenna. For polarization matched antennas, alignment is necessary for maximum directional radiation. In two antenna method Friis transmission formula can be written as

$$(G_{ot}) + (G_{or}) = 20 \log_{10} \left(\frac{4\pi R}{\lambda} \right) + 10 \log_{10} \left(\frac{P_r}{P_t} \right) \quad (4.1)$$

Where

$(G_{ot})_{dB}$ =gain of the transmission antenna (dB)

$(G_{or})_{dB}$ =gain of the receiving antenna (dB)

P_r =received power (W)

P_t =transmitted power (W)

R =antenna separation (m)

λ =operating wavelength(m)

If the transmitting and receiving antennas are identical ($G_{ot} = G_{or}$) then above Eqn.(4.1) reduces to

$$(G_{ot})_{dB} = (G_{or})_{dB} = \frac{1}{2} \left[20 \log_{10} \left(\frac{4\pi R}{\lambda} \right) + 10 \log_{10} \left(\frac{P_r}{P_t} \right) \right] \quad (4.2)$$

By measuring R, λ and the ration of P_r / P_t , the gain of the antenna can be obtained. The system is simple and the procedure is straight forward. Gain of the designed VCLA is computed by two antenna method at various frequencies. A plot of the gain versus frequency is shown in Fig 4.9. It is seen that above 300 MHz and below 600MHz the gain of the VCLA is almost constant. Thus the newly developed antenna can be considered as a frequency independent antenna above 300MHz and below 600MHz. Above 600 MHz the pattern of the antenna is also be distorted.

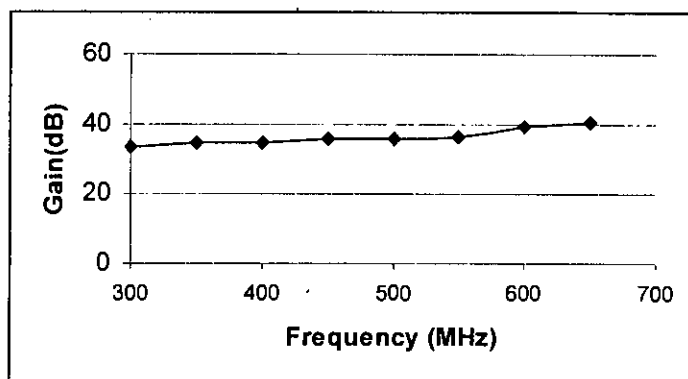


Fig.4.9 Comparison of Gain vs. Frequency at 3 m distance.

4.6.3 Directivity

The directivity of VCLA is higher than those of the other EMC antennas. If the different types of loss is neglected the directivity of the antenna is also 33 at the frequency 300 MHz

4.7 SE MEASUREMENT

The frequency range covered from 300 MHz to 600MHz for most of the samples. However, due, mainly, to the calibration inaccuracies at frequencies lower than 300 MHz, it was not possible to get very accurate SE data during on-line measurements, thus the lower range of frequency was selected to be 300MHz for on-line measurements. Meanwhile, above 660 MHz causing distortions to the test field. Thus the device is incapable of simulating standard high impedance field about that frequency.

4.7.1 Test Samples

A wide variety of conductive composite materials is available as mentioned earlier. Attempts have been made to investigate the SE values of each type. A few samples of surface metallized plastics were chosen. Five different types of samples such as Regularly filled (by copper) Composite Plastic (RFCP), Randomly filled (by copper) Composite plastic, Regularly filled (by copper) Square Loop Composite Plastic, Aluminium sheet and Aluminium Foil are chosen as samples for SE measurement. Samples are described in following paragraphs.

A sample of Aluminium Foil is shown in Fig.4.10(a) specially made, by pasting aluminium microfilm on a polythene paper using super adhesive glue was taken as one kind of metal plated polythene. The thickness of aluminium foil used was $2.5 \mu\text{m}$. This is then attached with a thick paper for ease handling.

Regularly Filled (by copper) Composite Plastic (RFCP) is a regular array of thin copper strips was developed on a printed circuit board (PCB) as shown in Fig 4.10(b). Because of the unavailability of large size PCBs, a $30\text{cm} \times 30\text{ cm}$ board was used (the selection of this particular size is dictated by the size of the diameter of the cone of the VCLA). The reflection coefficient of this array depends on several factors such as inter element separation, angle of incidence and type of the incident wave. Element size was selected to be 5.8 cm long and 1.5 cm wide.

Regularly Filled (by copper) Square Loop Composite Plastic was another type of sample which is prepared with a regular square loop of copper strips on a PCB as shown in Fig 4.10(c). The perimeter of a square loop is equal to the length of the copper strip of RFCP and the width of the loop is also same. Hence the total area of metal on the PCB was as RFCP printed circuit board.

Randomly filled (by copper) Composite Plastic was another sample which is prepared with a random distribution of the copper strips on a same size ($30 \times 30\text{ cm}$) PCB and is

shown in Fig 4.10(d). The dimension of each element and the total number of elements were the same as RFCP.

Aluminium Sheet was used as another sample as shown in Fig 4.10(e). The size of the sheet was also 30×30 cm and thickness of the aluminium sheet was 0.7mm.

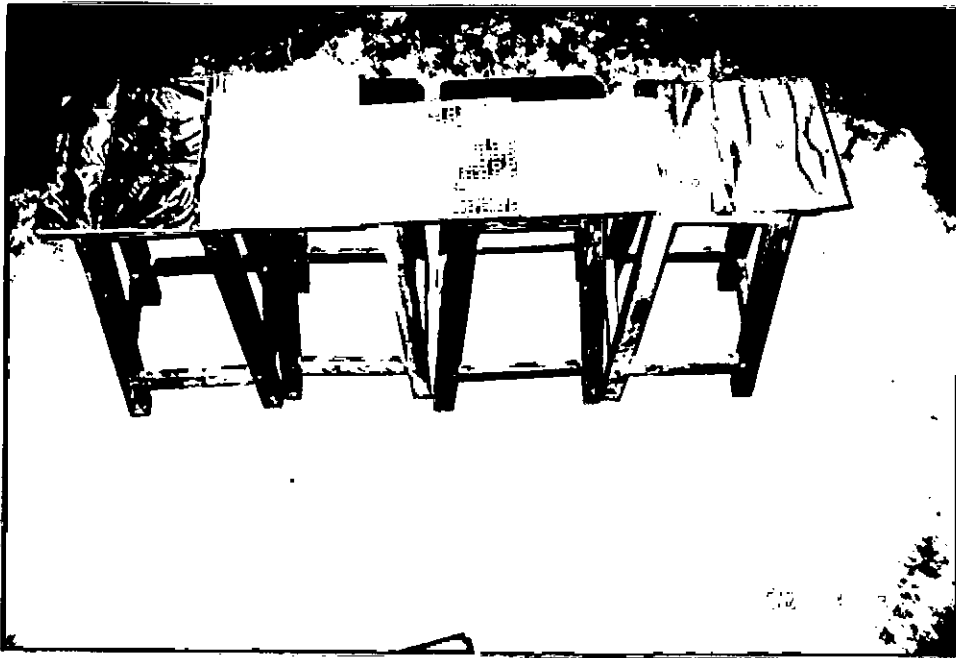


Fig. 4.10 Photograph of test samples (a) Aluminium foil, (b) Regularly filled composite plastic, (c) Regularly filled square loop composite plastic, (d) Randomly filled composite plastic and (e) Aluminium sheet.

4.7.2 Measurement of SE of the Test Samples

At first two VCLAs are kept into face to face position in a very small distance between them as shown in Fig 4.11. Then the RF signal of known strength is fed into the

transmitting antenna from a signal generator and received the RF signal by the receiving antenna. The strength of the received signal is then measured by a spectrum analyzer.

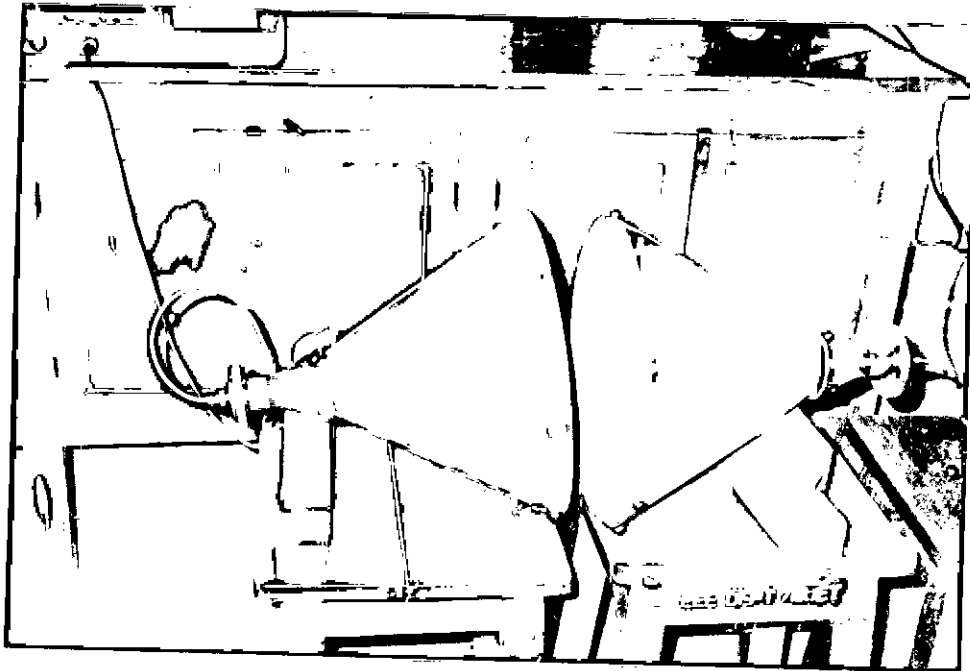


Fig 4.11: Measurement of signal strength without MUT.

Now the test sample is passed through the antenna apertures in such a position that the test sample is not capable to connect the antenna one with other which makes a short circuit as shown in Fig 4.12. The signal strength of received signal is then measured. Subtracting the result from the previous one and it is the expected Insertion Loss (IL) or Shielding Effectiveness of that sample. The SE at different frequencies is then measured.

Subtracting the result from the previous one and it is the expected Insertion Loss (IL) or Shielding Effectiveness of that sample. The SE at different frequencies is then measured.

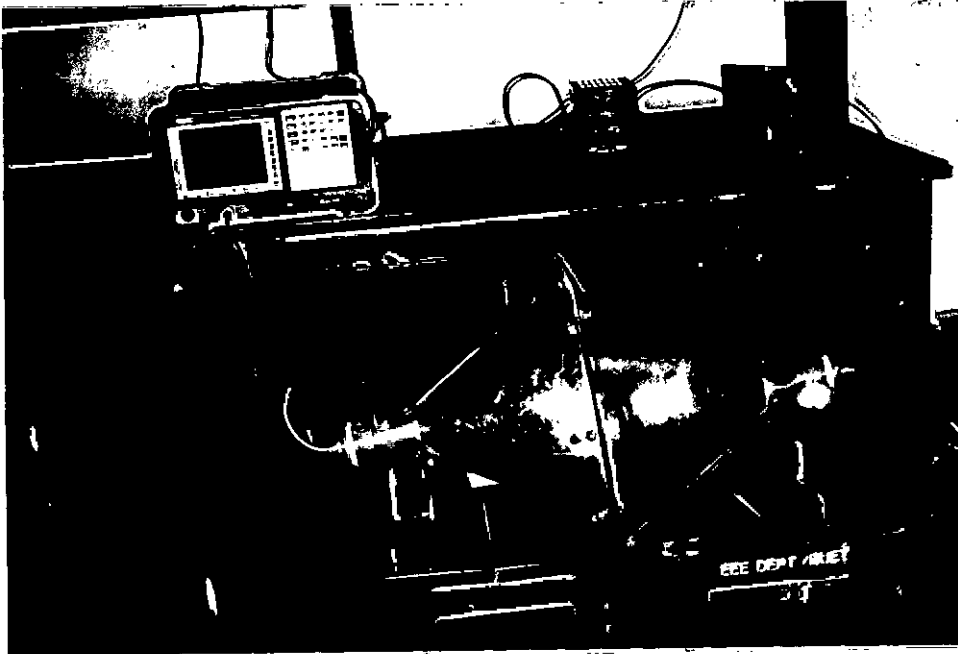


Fig.4.12: Measurement of signal strength with MUT.

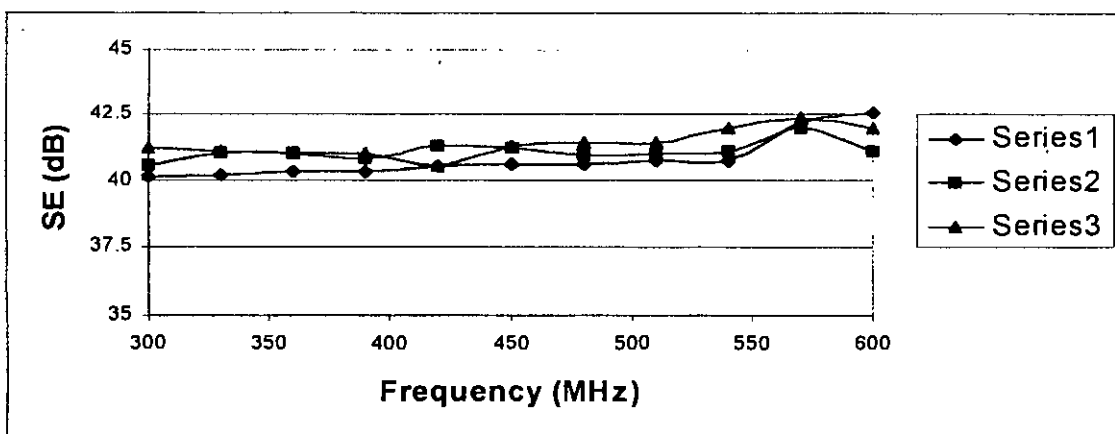


Fig 4.13 Variation of SE values of different types of conductive plastics (Series 1 for Array of regularly filled square loops, series 2 for array of regularly filled dipoles and series 3 for array of irregularly filled dipoles)

It is shown from Fig.4.13 that the SE of different types of conductive plastic substrates are almost constant at various frequencies (below 550MHz) which is the expected result of this present work. All SE values of the conductive plastics are in between 41.5 dB to 42.7dB. Due to beyond the scope of this work the theoretical SE values cannot be

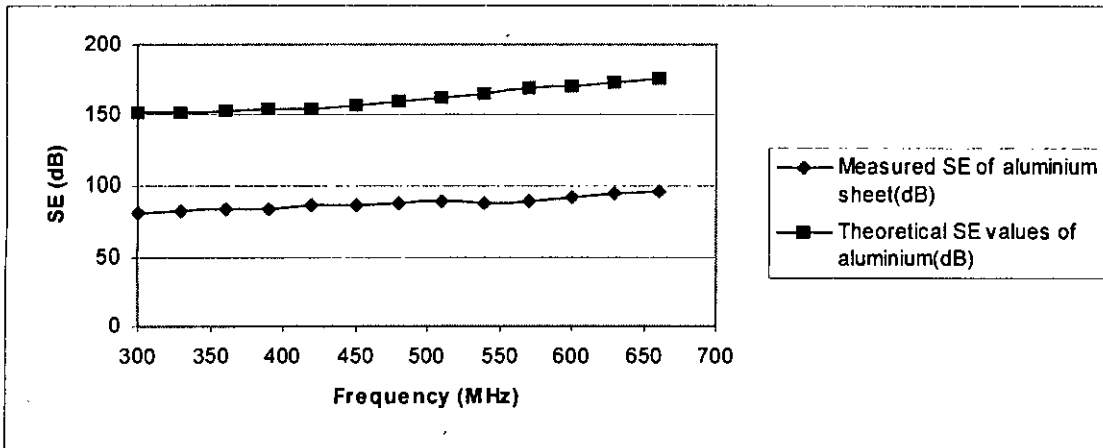


Fig 4.14 Comparison of SE of a aluminium sheet between measured SE values and theoretically calculated SE values.

calculated. From 4.14 it is observed that the SE values of aluminium sheet are varied with the theoretical values. It also may due to the non-standard measurement. It is found from the Fig 4.15 that the SE values of aluminium foil is almost constant which is our expected result. The variation with the theoretical result may due to the non-standard environment.

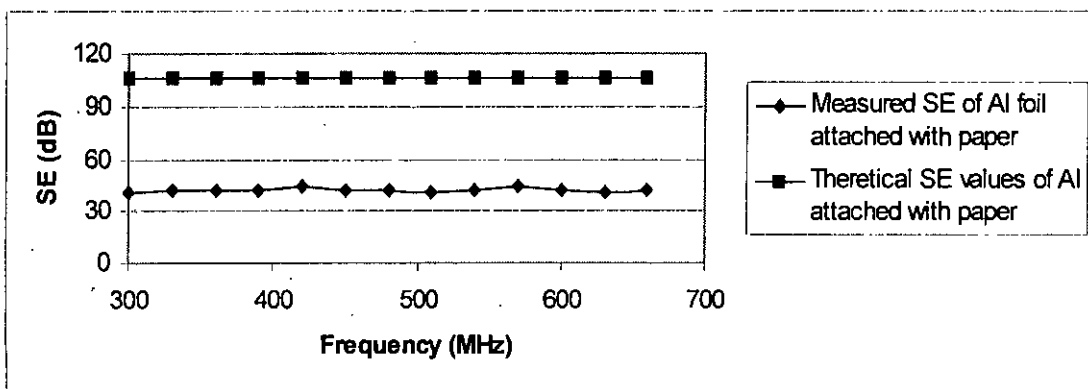


Fig.4.15 Comparison of SE values of a aluminium foil between measured values and theoretically computed values.



CHAPTER 5

CONCLUSION AND RECOMMENDATION OF FUTURE WORK



CONCLUSION



RECOMMENDATION FOR FUTURE WORK

CHAPTER - 5

CONCLUSION AND RECOMMENDATION FOR FUTURE WORK

5.1 CONCLUSION

An EMC antenna, namely V-Conical Lens Antenna (VCLA) is developed to measure the SE of planar sheet like materials during the production cycle. Developed VCLA consists of mainly two parts: (a) V-Conical Antenna and (b) Lens antenna. The lens antenna is used to transform the spherical wavefront generated by VCA into the plane wavefront.

The size of the antenna is dictated chiefly by the sheet width of the MUT. The feeding arrangement of the VCLA is such that the centre stud of the co-axial N-connector can be employed as a monopole antenna protruding into the cone to feed it and this is the usual procedure of the feeding wave guides. The electromagnetic field equations are solved by conformal mapping. The plano-convex lens is designed and constructed according to Fermat's principle. SE of different kinds of planar sheet like materials are measured and these are then compared with the theoretical values.

Some important features of newly developed VCLA alongwith theoretical background have been described in this work for better understanding of the salient features of developed antenna. The radiation pattern, directivity and gain of developed antenna are determined analytically and then compared with the measured result. The analytical determination of plane wave SE values of planar sheet like materials, film-coated plastic substrate, regularly filled array of dipoles and regularly filled square loop composite plastics have been presented in this work. The measurement of SE values for such kind of materials are then performed.

The radiation pattern of developed antenna is almost similar to that obtained from theoretical model except some weak field is found in the shadow region during measurement. The maximum power is observed at $\theta = 30^\circ$ in most of the case which is also consistent with the theoretical result. The gain at different frequencies is almost constant. Size and shape of the developed antenna have been selected in such a way which ensures the maximum radiated power, maximum gain and maximum directivity within the EMC frequency range.

In this work it has been assumed that the developed antenna holds the reciprocity theorem. Thus two VCLA have been used to measure the radiation pattern, where one acts as transmitting antenna and other acts as a receiving antenna. The developed antenna produce the desired field in a quasi-shielded environment requiring some calibration factors to be introduced into the test results to obtain the reliable SE data. Special measurements are thus essential to estimate appropriate correction factors and these can be introduced prior to recording the test results in course of automated measurement. Plane wave SE data differs widely due to reflection, absorption and successive re-reflections inside the MUT sheets.

97314
In few cases the results are distorted due to the non-standard environment. Open site location and anechoic chamber are required for any type of EMC measurement. Because the anechoic materials absorbs the incident EM energy on the wall, ceiling and floor from source within the chamber and then provides a nearly reflection free enclosure. So lack of anechoic chamber is another factor to influence the measurement. Edge diffraction is an additional factor to influence the measurement. Because capacitance may be grown between adjacent antennas when SE is measured.

5.2 RECOMMENDATION FOR FUTURE WORK

The following recommendations are made to carry out the future work:

- (1) As we said in chapter-1 that the SE of different planar sheet like materials will be measured during the production process. Due to the lack of on-line facilities measurement was not performed during the production process. But it will be very interesting work if the measurement will be done during the production process.
- (2) In this present research, there is no standard antenna. The measurement is done by considering one antenna as reference which are newly developed. Hence without calibration of antenna the measurement is performed. So, standard antenna and standard test site is required to calibrate the antenna.
- (3) In the solution of field equation, Moment Method (MM) or Finite Element Method may be introduced for full wave analysis of the antenna.

APPENDIX A

EVALUATION OF SHIELDING EFFECTIVENESS OF A PLANAR SHEET

The Shielding Effectiveness of a planar sheet may be evaluated from well-known two-wire transmission line equations [1]. From these transmission line equations, the impedance and output fields normal to an infinite planar sheet of thickness l can be written as

$$Z = \eta \frac{Z(l) \cosh \gamma l + \eta \sinh \gamma l}{\eta \cosh \gamma l + Z(l) \sinh \gamma l} \quad (\text{A.1})$$

$$H(l) = \frac{\eta}{\eta \cosh \gamma l + Z(l) \sinh \gamma l} H(0) \quad (\text{A.2})$$

$$E(l) = \frac{Z(l)}{Z(l) \cosh \gamma l + \eta \sinh \gamma l} E(0) \quad (\text{A.3})$$

Where, $Z(l)$ is the impedance looking to the right of the plane $x = l$

η is the intrinsic impedance of the sheet materials which can be expressed as

$$\begin{aligned} \eta &= \sqrt{\frac{j\omega\mu}{\sigma}} \\ &= (1+j) \sqrt{\frac{\pi\mu f}{\sigma}} \end{aligned}$$

Where μ , σ , f are the magnetic permeability, electrical conductivity and operating frequency respectively. The propagation constant

$$\gamma = \alpha + j\beta \quad (\text{A.4})$$

Where, α is the attenuation constant

β is the phase constant

If $Z(l) \neq \eta$, the reflection occurs at the boundary $x = l$. At this plane, let E^i , H^i be the incident electric fields and magnetic fields; E^r , H^r the reflected fields and E^t , H^t the transmitted fields as shown in Fig 2.1.

Since the fields are continuous across the plane

$$E^i + E^r = E^t, \quad H^i + H^r = H^t \quad (\text{A.5})$$

The reflected wave travels back to the source impedance for a sheet with a matched impedance at the plane $x=0$.

Thus

$$E^i = \eta H^i, \quad E^r = -\eta H^r, \quad E^t = Z(l) H^t \quad (\text{A.6})$$

By putting Eqn.(A.6) into Eqn.(A.5), the following expressions are obtained for reflection coefficients:

$$q_E = \frac{E^r}{E^i} = \frac{Z(l) - \eta}{Z(l) + \eta} = \frac{k - 1}{k + 1} \quad (\text{A.7})$$

$$\text{where } k = \frac{Z(l)}{\eta}$$

$$q_H = \frac{H^r}{H^i} = \frac{\eta - Z(l)}{\eta + Z(l)} = \frac{1 - k}{1 + k} \quad (\text{A.8})$$

$$q_E = -q_H \quad (\text{A.9})$$

The transmission coefficients:

$$p_E = \frac{E^t}{E^i} = \frac{2Z(l)}{\eta + Z(l)} = \frac{2k}{1 + k} = 1 + q_E \quad (\text{A.10})$$

$$p_H = \frac{H^t}{H^i} = \frac{2\eta}{\eta + Z(l)} = \frac{2}{1 + k} = 1 + q_H \quad (\text{A.11})$$

When two mismatched interfaces must be considered as in a planar sheet, the net transmission coefficient is the product of the transmission coefficients across the two boundaries. Hence

$$p = p_E = p_H = p_E(0) \cdot p_E(l) = p_H(0) \cdot p_H(l) = \frac{4k}{(1+k)^2} \quad (\text{A.12})$$

The reflection loss can be written in terms of transmission coefficient as

$$R = -20 \log_{10} |p| = 20 \log_{10} \frac{|1+k|^2}{4|k|} \quad (\text{A.13})$$

The reflection loss expressed in Eqn.(A.13) is on the basis that the reflected wave travels back to infinity or suffers sufficiently high penetration loss that successive re-reflections may be neglected as in Fig.2.1(a).

Fig.2.1(b) is the more general case whereby successive re-reflections may not be neglected. For this case, the transmission coefficients across the sheet can be written as

$$T_H = \frac{H(l)}{H^i} = \frac{H(l)}{H(o)} \cdot \frac{H(o)}{H^i} \quad (A.14)$$

$$T_E = \frac{E(l)}{E^i} = \frac{Z(l)}{Z_w} \cdot \frac{H(l)}{H^i} = \frac{Z(l)}{Z_w} T_H \quad (A.15)$$

Where, $E(o)$, $H(o)$, $E(l)$, $H(l)$ are the actual values at interfaces o and l , respectively, with reflection taken into account; Z_w is the impedance of the incident wave. By the use of Eqn (A.4) for sheets of thickness 0 and l the following ratios are obtained.

$$\frac{H(l)}{H(o)} = \frac{\eta}{\eta \cosh rl + Z(l) \sinh rl} \quad (A.16)$$

$$\frac{E(l)}{E(o)} = \frac{Z(l)}{Z(l) \cosh rl + \eta \sinh rl} \quad (A.17)$$

From Eqn.(A.6)

Where, $Z(o)$ is the impedance at interface 0 looking into the sheet. By substituting this equations into (A.15) and performing some algebraic manipulation, the following formula is obtained:

$$\frac{H(o)}{H^i} = \frac{\eta Z_w}{Z_w + Z(o)} \quad (A.18)$$

$$\frac{E(o)}{E^i} = \frac{2Z(o)}{Z_w + Z(o)} \quad (A.19)$$

$$T_H = p_H (1 - q_H e^{-2rl})^{-1} e^{-rl} \quad (A.20)$$

$$\text{where, } p_H = \frac{4Z_w \eta}{(Z_w + \eta)[Z(l) + \eta]} \quad (A.21)$$

$$q_H = \frac{(Z_w - \eta)[Z(l) - \eta]}{(Z_w + \eta)[Z(l) + \eta]} \quad (A.22)$$

when,

$$Z(l) = Z_w$$

$$p = \frac{4k}{(k+1)^2} \quad (A.23)$$

$$q = \frac{(k-1)^2}{(k+1)^2} \quad (A.24)$$

Where, k is the ratio of characteristic impedance Z_w / η

Then, $T_H = T_E$ or

$$T = p(1 - qe^{-2rl})^{-1} e^{-rl} \quad (A.25)$$

By definition the total shielding effectiveness is

$$S = -20 \log_{10} |T| \quad (A.26)$$

$$\begin{aligned} &= 20 \log_{10} \left| \frac{(1 - qe^{-2rl}) e^{rl}}{p} \right| \\ &= 20 \log_{10} |e^{rl}| - 20 \log_{10} |p| + 20 \log_{10} |1 - qe^{-2rl}| \end{aligned} \quad (A.27)$$

Expression (A.27) is the complete formula for shielding effectiveness of a single shield where the first term represents the absorption loss, the second term represents the reflection loss and the third term represents the correction term for successive re-reflections.

For a metallic sheet of thickness t the absorption loss and reflection loss are given as [15]:

$$A = 8.686 \alpha t \sqrt{\pi \mu \sigma} \quad (A.28)$$

and

$$R = 20 \log_{10} \frac{|1 + k|^2}{4|k|} \quad (\text{A.29})$$

The positive or negative correction term which need not be taken into account when A is more than 15dB. It is caused by the reflecting waves inside the shielding barrier and is calculated in dB. When a metallic barrier has an absorption loss (A) of less than 15 dB, it is designed as “electrically thin”.

APPENDIX B

USE OF METALLIC- FILM COATING ON PLASTIC SUBSTRATE

A conductor of high conductivity and low permeability has low intrinsic impedance [16]. When a radio wave propagates from a medium of high intrinsic impedance into a medium of low intrinsic impedance, the reflection coefficient is high. From electromagnetic plane wave theory in the far field, high attenuation occurs in a medium made of material having high conductivity and low permeability. Good conductors, such as gold, silver, copper, aluminium, have high conductivity and are often used as the material for attenuating electromagnetic energy. Microwave radiation attenuation by a metallic film coating on substrate consists of three parts as discussed in Appendix-A. These are as follow:

Absorption Loss A: The propagation constant γ for a uniform plane wave in a good conducting material is given as

$$\gamma = \alpha + j\beta = (1+j)\sqrt{(\pi f \mu \sigma_f)} \quad \text{for } \sigma_f \gg \omega \epsilon \quad (\text{B.1})$$

If the plastic substrate is assumed to be a non-absorbing material, the absorption (loss A) of the metallic-film coating on a substrate is related only to the thickness t of the coated film and the attenuation α as shown:

$$\begin{aligned} A &= 20 \log_{10} e^{\alpha t} \\ &= 20(\alpha t) \log_{10} e \\ &= 20(0.4343) (\alpha t) \\ &= 8.686t) \sqrt{(\pi f \mu \sigma_f)} \quad \text{dB} \end{aligned} \quad (\text{B.2})$$

where

- t = thickness of the film coating in meters
- μ = permeability of the film in henrys per meter
- f = frequency in hertz
- σ_f = conductivity of the coated film in mhos per meter

Since the thickness of the coated film is very thin – for example, 100 \AA at most the absorption loss A is very small and can be ignored.

Reflection loss R: The reflection loss R due to the multiple boundaries of the substrate glass coated with a metallic film can be analyzed by means of the energy-transmission theory and it is expressed as

$$R = -20 \log \frac{2|\eta_f|}{|\eta_a + \eta_f|} - 20 \log \frac{2|\eta_g|}{|\eta_f + \eta_g|} - 20 \log \frac{2|\eta_a|}{|\eta_g + \eta_a|} \quad (B.3)$$

$$= 20 \log \frac{|\eta_a + \eta_f| |\eta_f + \eta_g| |\eta_g + \eta_a|}{8 |\eta_f| |\eta_g| |\eta_a|} \quad dB \quad (B.4)$$

Where η_f =intrinsic impedance of the coated metallic film

η_g = intrinsic impedance of the glass substrate

η_a = intrinsic impedance of air or free space = 377Ω

The intrinsic impedance of the coated metallic film is given as

$$|\eta_f| = \left| (1 + j) \sqrt{\frac{\mu\omega}{2\sigma_f}} \right| = \sqrt{\frac{\mu\omega}{\sigma_f}} \quad (B.5)$$

and the intrinsic impedance of a glass substrate is expressed as

$$\eta_g \approx \frac{\eta_a}{\sqrt{\epsilon_r}} = \frac{377}{\sqrt{3.78}} = 194 \Omega \quad \text{for } \sigma_g \ll \omega\epsilon_g \quad (B.6)$$

where σ_g = about 10^{-12} mho/m is the conductivity of the glass substrate

$\epsilon_g = 4.77 \times 10^{-11}$ F/m is the permittivity of the glass substrate

$\epsilon_r = 3.78$ is the relative permittivity of the glass substrate

Substituting the values of the intrinsic impedances η_f , η_g , and η_a in Eqn. (B.4) yields the reflection loss as

$$R \approx 20 \log \left[28.33 \sqrt{\frac{\sigma_f}{\mu f}} \right] = 88 + 10 \log \left(\frac{\sigma_f}{f} \right) \quad \text{dB} \quad (\text{B.7})$$

Correction Term C: For very electrically thin film, the value of the absorption loss A is much less than 10 dB and the correction term is given as[16]:

$$C = 20 \log | 1 - \rho 10^{-A/10} (\cos\theta - j \sin\theta) | \quad (\text{B.8})$$

Where

$$\rho = \left(\frac{\eta_f - \eta_a}{\eta_f + \eta_a} \right)^2 \approx 1 \quad \text{for} \quad \eta_a \gg \eta_f$$

$$\theta = 3.5 t \sqrt{f \mu \sigma_f}$$

Over the frequency range of 100 MHz to 40GHz, the angle θ is much smaller than 1° so that $\cos\theta \approx 1$ and $\sin\theta \approx \theta$. Thus the correction term of Eqn.(B.8) can be simplified to

$$C \approx 20 \log [3.5 t \sqrt{(f \mu \sigma_f)}] = -48 + 20 \log [t \sqrt{(f \sigma_f)}] \quad \text{dB} \quad (\text{B.9})$$

Finally, the total microwave radiation attenuation by a metallic coating on a glass substrate, defined in Eqn.(A.26) in the far field, becomes

$$\text{Attenuation} = 40 - 20 \log_{10}(R_s) \quad (\text{B.10})$$

Where $R_s = 1/t\sigma_f$ Ω/square

It is interesting to note that the microwave radiation attenuation due to the coated metallic film on a substrate in the far field is independent of frequency and is related only to the surface resistance of the coated metallic film.

SE OF THE ARRAY OF DIPOLE

SE consists of absorption loss (A), reflection loss (R) and successive re-reflection loss (B) of the RECP. For a doubly periodic array of dipoles in an equivalent homogeneous medium (ϵ_{re}) as shown in Fig.2.2, there will be no absorption loss due to the use of strip like filler. Successive reflection loss is very negligible. SE of the array of dipoles in a homogeneous medium having an effective dielectric constant (ϵ_{re}) can then be expressed as follow

$$SE = R \quad \text{dB} \quad (C.1)$$

Reflection loss (R) can be determined by multiplying the incident power with the reflection coefficient (R').

Reflection coefficient of the array of dipoles

A plane wave, which is incident on the periodic array of dipoles as shown in Fig 2.2 is considered to be linearly polarized in z direction. The direction of propagation lies in the x-y plane, making an angle ϕ_1 with negative y-axis as shown in Fig 2.2. The specular reflection for such an array can be expressed as [17].

$$R' = \frac{K(l_\lambda, l_e, Z_L, Z_A) l^4 \sec^2 \phi_i}{[D_x D_z (Z_A + Z_L)]^2} \quad (C.2)$$

where

$$K(l_\lambda, l_e, Z_L, Z_A) = 3600 \frac{\left| F_{e1} - \left(\frac{Z_L}{Z_A} \right) F_{e2} \right|^2 F_{e3}^2}{\pi^2 l_\lambda^4}$$

$$F_{e1} = \frac{\sin \beta l - \beta l_e \cos \beta l_e}{1 - \cos \beta l_e}$$

$$F_{e2} = \frac{1}{\sin \beta l_e} [1 - \cos \beta l_e - F_{e1} \sin \beta l_e]$$

and

$$F_{e3} = \frac{\cos \beta \Delta l - \cos \beta l_e}{\sin \beta l_e}$$

In the above equations, $l_\lambda = l/\lambda$, where λ is the wave length of the incident wave, $\Delta l = l_e - l$, $\beta = 2\pi/\lambda$ is the phase constant and Z_A is the driving point impedance of each element and Z_L is the impedance loaded in each dipole. D_x is the distance between two identical elements, D_z is the distance between two adjacent rows. l and l_e is the half of the length of element and effective length of the element respectively.

The driving point impedance of the array can be written as [17].

$$Z_A = \sum_{r'=-R'}^{R'} \sum_{k=-K}^K \varepsilon_k Z_{rk} \cos(\beta D_x k \sin \phi_i) \quad (C.3)$$

where, ε_k is the Neumann factor defined by

$$\begin{aligned} \varepsilon_k &= 1 \quad \text{for } k = 0 \\ &= 2 \quad \text{for } k \neq 0 \end{aligned}$$

SE OF THE ARRAY OF SMALL SQUARE LOOPS

For the array of small square loops in a homogeneous medium having an effective dielectric constant (ϵ_{er}), reflection loss (R) as well as absorption loss (A) will be available. There will be no successive reflection loss (B) due to the use of thin square loop like filler. SE of such RFCP can be expressed as

$$SE = A + R \quad \text{dB} \quad (D.1)$$

Where, A is the absorption loss and R is the reflection loss. Reflection coefficient and absorption loss has been evaluated in the following subsections.

Reflection coefficient and absorption loss of the array of small square loops

A doubly periodic array of small square loops in a homogeneous medium having an effective dielectric constant (ϵ_{er}) is shown in Fig.2.3. In this case for computing the reflection coefficient, this type of array configuration has been considered as a combination of vertical (z-directed) array and horizontal (x-directed) array of dipoles by satisfying the following conditions.

- number of rows and number of columns of the vertical and horizontal dipole array must be even and equal i. e. $r_1' = r_2'' = r'$ and $k_1 = k_2 = k$.
- length of element for both the vertical and horizontal arrays must be equal and should be electrically small.
- spacing between two adjacent array element in the case of vertical array (i. e. z-directed) will be as follow: $D_{x2} = 2l$ and $D_{z2} = 2D_{z1} = 4l$
- spacing between two adjacent array element in the case of horizontal array (x-directed) will be as follow: $D_{x2} = 2D_{x1} = 4l$ and $D_{z2} = 2l$

The reflection coefficient of the array of small square loops as shown in Fig.2.3 will then be

$$\mathbf{R}' = \mathbf{R}'_1 + \mathbf{R}'_2 \quad (\text{D.2})$$

Where \mathbf{R}'_1 is the reflection coefficient of the vertical array of dipoles and \mathbf{R}'_2 is the reflection coefficient of the horizontal array of dipoles which are given in following subsection.

In the case of square loop there will be no free charge on the loop i.e. ρ_l . Thus the scalar potential term is zero and the electric field will then be only due to the vector potential. The electric field then becomes as [18]

$$E_z = \frac{\omega \mu I_1}{8\pi} \int_{-l}^{+l} \left(\frac{e^{-j\beta(z_1+r)} - e^{j\beta(z_1-r)}}{r} \right) dz_1 \quad (\text{D.3})$$

Reflection coefficient of vertical array

Reflection coefficient of vertical array (i.e. z directed dipoles) is determined in a similar manner as that of the array of z directed dipoles. The mutual impedance of the vertical array can be expressed as

$$Z_{1r'k} = -\frac{\omega \mu}{8\pi \sin^2 \beta l_e} \int_{r'D_{z1}}^{r'D_{z1}+2l} [\sin \beta(l_e - |z|) \int_0^{2l} \left(\frac{\exp\{-j\beta(\Delta z' + r_1)\} - \exp\{j\beta(\Delta z' - r_1)\}}{r_1} \right) dz_1] dz \quad (\text{D.4})$$

where

$$r_1 = [(kD_{z1})^2 + (z - z_1)^2]^{1/2}$$

$z_1 = z$ coordinate on the dipole

$r' =$ number of rows which varies from $-R''$ to $(R''+1)$.

$$\Delta z' = l_e - |z_1|$$

k = number of columns which varies from $-K$ to $(K+1)$.

Driving point impedance of vertical array is determined as

$$Z_{1A} = \sum_{r'=-R'}^{R'+1} \sum_{k=-K}^{K+1} \epsilon_k Z_{1r'k} \cos(\beta D_{x1} k \sin \phi_i) \quad (D.5)$$

Reflection coefficient of the vertical array then yields as

$$R' = \frac{K_1(l_\lambda, l_e, Z_L, Z_{1A}) l^4 \sec^2 \phi_i}{[D_{x1} D_{z1} (Z_{1A} + Z_L)]^2} \quad (D.6)$$

where

$$K_1(l_\lambda, l_e, Z_L, Z_A) = 3600 \frac{\left| F_{e1} - \left(\frac{Z_L}{Z_{1A}} \right) F_{e2} \right|^2 F_{e3}^2}{\pi^2 l_\lambda^4} \quad (D.7)$$

F_{e1} , F_{e2} , F_{e3} are as given in Appendix- C.

Reflection Co-efficient of the Horizontal Array

Reflection coefficient of the horizontal array (i.e. x - directed dipoles) is determined in a similar way. The mutual impedance of the horizontal array can be expressed as

$$Z_{2r'k} = -\frac{\omega \mu}{8\pi \sin^2 \beta l_e} \int_{r'D_{x1}}^{r'D_{x1}+2l} [\sin \beta(l_e - |x|)] \int_0^{2l} \left(\frac{\exp\{-j\beta(\Delta x' + r_2)\} - \exp\{j\beta(\Delta x' - r_2)\}}{r_2} \right) dx_1 dx \quad (D.8)$$

Where

$$r_2 = [(kD_{z2})^2 + (x - x_i)^2]^{1/2}$$

x_i = x coordinate in the dipole

$$\Delta x' = l_e - |x_l|$$

Driving point impedance of horizontal array yields as

$$Z_{2A} = \sum_{r'=-R'}^{R'+1} \sum_{k=-K}^{K+1} \epsilon_k Z_{2r'k} \cos(\beta D_{z2} k \cos \phi_i) \quad (\text{D.9})$$

Reflection coefficient of the horizontal array then becomes as

$$R_2' = \frac{K_2(l_\lambda, l_e, Z_L, Z_{2A}) I^4 \operatorname{cosec}^2 \phi_i}{[D_{x2} D_{z2} (Z_{2A} + Z_L)]^2} \quad (\text{D.10})$$

Where

$$K_2(l_\lambda, l_e, Z_L, Z_{2A}) = 3600 \frac{\left| F_{e1} - \left(\frac{Z_L}{Z_{1A}} \right) F_{e2} \right|^2 F_{e3}^2}{\pi^2 l_\lambda^4} \quad (\text{D.11})$$

Absorption loss of the array of small square loops

Voltage induced in the loop due to the incident field can be expressed as follow [3]

$$V_{11} = \frac{1}{I_1} \int_0^{2l} I_z E_z dz \quad (\text{D.12})$$

The current (I_z) at a distance z from the origin is given as [18]

$$I_z = I_1 \sin \beta z \quad (\text{D.13})$$

Substituting Eqn.(D.3) and Eqn.(D.13) into the Eqn.(D.12) yields

$$V_{11} = \frac{\omega \mu}{8\pi} \int_0^{2l} \left[\sin \beta z \int_0^{2l} \left(\frac{e^{-j\beta(z_1+r)} - e^{j\beta(z_1-r)}}{r} \right) dz_1 \right] dz \quad (\text{D.14})$$

Eqn.(D.14) is restricted for the case where each side of the square loop is equal to the odd multiple of the half wavelength. For the case of the loop sides of any length Eqn. (D.14) becomes

$$V_{11} = \frac{\omega\mu}{8\pi \sin^2 \beta l_e} \int_0^{2l} \left[\sin \beta z \int_0^{2l} \left(\frac{e^{-j\beta(z_1+r)} - e^{j\beta(z_1-r)}}{r} \right) dz_1 \right] dz \quad (D.15)$$

$$R_L = \frac{L}{2a} \sqrt{\frac{f\mu_0}{\pi\sigma}} \quad (D.16)$$

By small loop approximation (i.e. loop perimeter $\ll \lambda$), loop loss resistance is found as follow [3]

Where

L = loop perimeter, m

a = wire (conductor or dipole) radius, m

σ = conductivity of the loop material, mhos/m

Absorption loss in a loop will then be as

$$A_L = \frac{V_{11}^2}{R_L} \quad (D.17)$$

Total absorption loss of the array of small square loops can be expressed as :

$$A = 10 \log_{10}(A_L M) \quad \text{dB} \quad (D.18)$$

Where M is the total number of loops in the array.

REFERENCES

- [1] B.Schulz, C.Plantz and R. Brush, "Shielding Theory and Practice", *IEEE Trans. on EMC*, vol.30, no.3, pp. 187-201 .August,1988.
- [2] Clayton R. Paul, *Introduction to Electromagnetic Compatibility*, pp. 265-274, John Wiley & Sons, Inc. New York.
- [3] J. D. Krauss, *Antennas*, McGraw-hill, NY, pp.257, 422-430,1988.
- [4] S. A. Schelkunoff, *Electromagnetic Waves*, New York: Van Nostrand, pp. 303-315,1943.
- [5] R. W Simpson, Jr., "Flexible laminates for use in EMI shielding applications", *IEEE Electrical Insulation Magazine*, vol. 4. no. 1, pp. 11-13, Jan./Feb. 1988.
- [6] H.Rahman, P. K. Saha, J. Dowling and T.Curran "Shielding effectiveness measurement techniques for EMI shielding", *IEE Colloquium on Screening of connectors, Cables and Enclosures*, pp.9/1-9/6, London, UK, 17 Jan.1992.
- [7] Peery F. Wilson, Mark T. J.W.Adams, "Techniques for measuring the electromagnetic shielding effectiveness of materials:Part-I:-Far-field source simulation", *IEEE Trans. on EMC*, vol.30, no.3, pp.239-250, August 1988.
- [8] MIL-STD-285, " Attenuation Measurements for enclosures, electromagnetic shielding, for electronic test purposes, method of", August 1956.

- [9] W. R. Scott, "A new technique for measuring the constitutive parameters of planar materials", *IEEE Trans. on IM*, vol.41, no. 5, pp. 639-645, Oct. 1992.
- [10] P.F.Wilson and M. T. Ma. "Shielding effectiveness measurements with a dual TEM cell", *IEEE Trans. on EMC*, vol. EMC-27, no.3, pp. 137-142. August 1985.
- [11] E. Hariya and U. Masahiro, "Instruments for measuring the shielding effectiveness", *IEEE international symposium on EMC*, Tokyo, Japan, pp.800-805, October 1984.
- [12] J. Catrysse, "A new test-cell for the characterisation of shielding materials in the far field", *IEEE proceedings of the 7th International Conference on EMC*, York, UK. pp.62-67, August 1990.
- [13] W. Graf and E.F. Vance, "Shielding effectiveness and electromagnetic protection", *IEEE Trans. on EMC*, vol.30,no.3, pp.289-293, Aug.1988.
- [14] G. Dike, "Electromagnetic Relationships Between Shielding Effectiveness And Transfer Impedance", *IEEE International Symp.on EMC*, Oct.1979.
- [15] Samuel Y. Liao, *Microwave Devices and Circuits*, Second Edition, PRENTICE-HALL, INC., Englewood Cliffs, New Jersey, 07632.
- [16] VASAKA, C. S., "Problems in shielding electrical and electronic equipment," *U.S. Naval Air Development Center. Johnsville, Pa., Rept No. NACD-EL-N5507*, June 1955 .
- [17] Benedikt A. Munk, P. G. Kouyoumjian and L. Peters Jr., "Reflection properties of periodic surfaces of loaded dipoles," *IEEE Trans. on Antennas and propagation*, vol. AP-19. no.5, pp.612-617, Sept.1971.
- [18] S.M.Shamim Hasan, "Evaluation of Shielding Effectiveness of a Regularly Filled Conductive Composite for Electromagnetic Shielding", *Post graduate thesis*, 1998.

[19] Hao-Ming Shen, Ronald W.P.King and Tai Tsun Wu, " V-Conical Antenna," *IEEE Trans. on Antennas and Propagation*, vol.36, pp. N0.11, pp.1519-1525, November,1988.

[20] R.L. Carrel, "The Characteristic Impedance of Two Infinite Cones of Arbitrary Cross-section," *IRE Trans. on Antennas and Propagation*, Vol. AP-6, pp.197-201, 1958.

[21] Constantine A. Balanis, *Antenna Theory Analysis and Design*, Second Edition, John Wiley & Sons, Inc. pp. 867-868.

[22] Hafizur Rahman, " Development of EMC antennas and their application in on-line SE measurement of conductive composite plastic materials," *A Ph. D. Thesis*, 1994.

